7936 *Macromolecules* **2010**, *43*, 7936–7949
DOI: 10.1021/ma1009319

Macromolecules
ARTICLE

Synthesis, Light-Emitting, and Two-Photon Absorption Properties of Platinum-Containing Poly(arylene-ethynylene)s Linked by 1,3,4-Oxadiazole Units

Thomas Goudreault,[†] Ze He,[‡] Yanhe Guo, Cheuk-Lam Ho,[‡] Hongmei Zhan,[‡] Qiwei Wang,[‡] Keith Yat-Fung Ho,[∥] Ka-Leung Wong,[‡] Daniel Fortin,[†] Bing Yao,[§] Zhiyuan Xie,[§] Lixiang Wang,[§] Wai-Ming Kwok,[∥] Pierre D. Harvey,*[,†] and Wai-Yeung Wong*[,‡]

[†]*Département de Chimie, Université de Sherbrooke, 2550 Boul. Université, Sherbrooke, PQ, J1K 2R1 Canada,* [‡]*Department of Chemistry and Centre for Advanced Luminescence Materials, Hong Kong Baptist University, Waterloo Road, Kowloon Tong, Hong Kong, P.R. China,* [§]*State Key Laboratory of Polymer Physics and Chemistry, Changchun Institute of Applied Chemistry, Chinese Academy of Sciences, Changchun 130022, P.R. China, and* [∥]*Department of Applied Biology and Chemical Technology, The Hong Kong Polytechnic University, Hung Hom, Hong Kong, P.R. China*

Received April 29, 2010; Revised Manuscript Received July 24, 2010

ABSTRACT: A series of soluble and thermally stable group 10 platinum(II) polyyne polymers of the type $[-C{\equiv}C-Pt(PBu_3)_2-C{\equiv}C-\mathbf{Ar}-\mathbf{Ox}-\mathbf{Ar}-]_n$ (where **Ox** = 1,3,4-oxadiazole; **Ar** = *p*-C_6H_4 or 2,7-dihexyl-9,9-fluorene) and $[-C{\equiv}C-Pt(PBu_3)_2-C{\equiv}C-\mathbf{Ar}-\mathbf{Ox}-\mathbf{Ar}-\mathbf{Ox}-\mathbf{Ar}-]_n$ (where **Ar** = 2,7-dihexyl-9,9-fluorene) along with their corresponding dinuclear model compounds $[Ph-Pt(PEt_3)_2-C{\equiv}C-\mathbf{Ar}-]_2-\mathbf{Ox}-$ (where **Ar** = *p*-C_6H_4 or 2,7-dihexyl-9,9-fluorene) and $[Ph-Pt(PEt_3)_2-C{\equiv}C-\mathbf{Ar}-\mathbf{Ox}-]_2-\mathbf{Ar}-$ (where **Ar** = 2,7-dihexyl-9,9-fluorene) were prepared and characterized. The regiochemical structure of the polymers has been ascertained by single-crystal X-ray analysis on the model compound $[Ph-Pt(PEt_3)_2-C{\equiv}C-p-C_6H_4-]_2-\mathbf{Ox}-$. The photophysical properties (absorption, excitation, emission, and nanosecond transient absorption spectra) of these metalated compounds in 2MeTHF at 298 and 77 K are reported. These findings are correlated by density functional theory (DFT) calculations. Geometry optimizations predict totally planar molecules for these metalated complexes and polymers, allowing better π-conjugation across the main chain. The ligands are strongly fluorescent but become also phosphorescent when the Pt atom is introduced in the backbone of the conjugated organometallic complexes and polymers. These emissions are assigned to $\pi\pi^*$ transitions in all cases involving the Pt d_{xy} orbitals. These Pt compounds exhibit two-photon absorption (2PA), and their 2PA cross sections (σ_2) have been determined. The potential of exploiting such metallopolymers for the design of electrophosphorescent polymer light-emitting devices (PLEDs) and their use as single-dopant for white PLEDs have also been discussed.

Introduction

The 1,3,4-oxadiazole (**Ox**) unit is still a very popular chromophore in organic small molecules and polymers for photonic devices, notably for organic (OLEDs) and polymer light-emitting diodes (PLEDs)[1] and photovoltaic cells.[2] Other applications were also reported such as electroluminescent colloidal inks,[3] nonlinear optical properties,[4] stable membrane in fuel cells,[5] corrosion protection,[6] and proton exchange.[7] Oxadiazole derivatives are well known for their high electron affinity values and excellent electron-transporting properties in organic multilayer electroluminescent diodes.[8] Therefore, various oxadiazole derivatives have been widely used as electron-transporting and hole-blocking materials in OLED devices.[9] The use of the **Ox** unit to form metal coordination polymers (where the coordination bonds occur via the N-lone pair) is also known,[10] but to our knowledge, there is no PLED investigation designed with them. Syntheses of conjugated organometallic acetylide complexes containing the **Ox** fragment in the backbone were only recently investigated.[11]

In organic polymers, acetylenic polymers[12] and fluorene derivatives[13] are used in many optoelectronic applications because of their thermal and chemical stability and their high emission quantum yields. The ease of modification and knowledge of the structure−property relationships of polyfluorene copolymers render the fluorene-functionalized compounds very attractive candidates in the design of new functional materials.[13] The fluorene structural moiety provides a rigidly planar biphenyl unit within the molecular backbone. Substituent derivatization at the C-9 position of the fluorene ring provides the prospect of controlling polymer properties such as solubility, emission wavelength, and processability and mediating potential interchain interactions in films.[14]

We now report the syntheses and characterization of a series of soluble and thermally stable group 10 platinum(II)-polyyne-conjugated polymers of the type $[-C{\equiv}C-Pt(PBu_3)_2-C{\equiv}C-\mathbf{Ar}-\mathbf{Ox}-\mathbf{Ar}-]_n$ (where **Ox** = 1,3,4-oxadiazole; **Ar** = *p*-C_6H_4 or 2,7-dihexyl-9,9-fluorene) and $[-C{\equiv}C-Pt(PBu_3)_2-C{\equiv}C-\mathbf{Ar}-\mathbf{Ox}-\mathbf{Ar}-\mathbf{Ox}-\mathbf{Ar}-]_n$ (where **Ar** = 2,7-dihexyl-9,9-fluorene) along with their corresponding dinuclear model compounds $[Ph-Pt(PEt_3)_2-C{\equiv}C-\mathbf{Ar}-]_2-\mathbf{Ox}-$ (where **Ar** = *p*-C_6H_4 or 2,7-dihexyl-9,9-fluorene) and $[Ph-Pt(PEt_3)_2-C{\equiv}C-\mathbf{Ar}-\mathbf{Ox}-]_2-\mathbf{Ar}-$ (where **Ar** = 2,7-dihexyl-9,9-fluorene; Chart 1). Their electronic spectra (absorption, excitation, emission, and nanosecond transient absorption spectra) and excited-state dynamics (fluorescence and phosphorescence lifetimes and quantum yields) were investigated in detail. The density functional theory (DFT) computations

*Corresponding authors. E-mail: (W.-Y.W.) rwywong@hkbu.edu.hk; (P.D.H.) Pierre.Harvey@USherbrooke.ca.

 Published on Web 09/16/2010

Chart 1. Chemical Structures of 1−9 in This Work

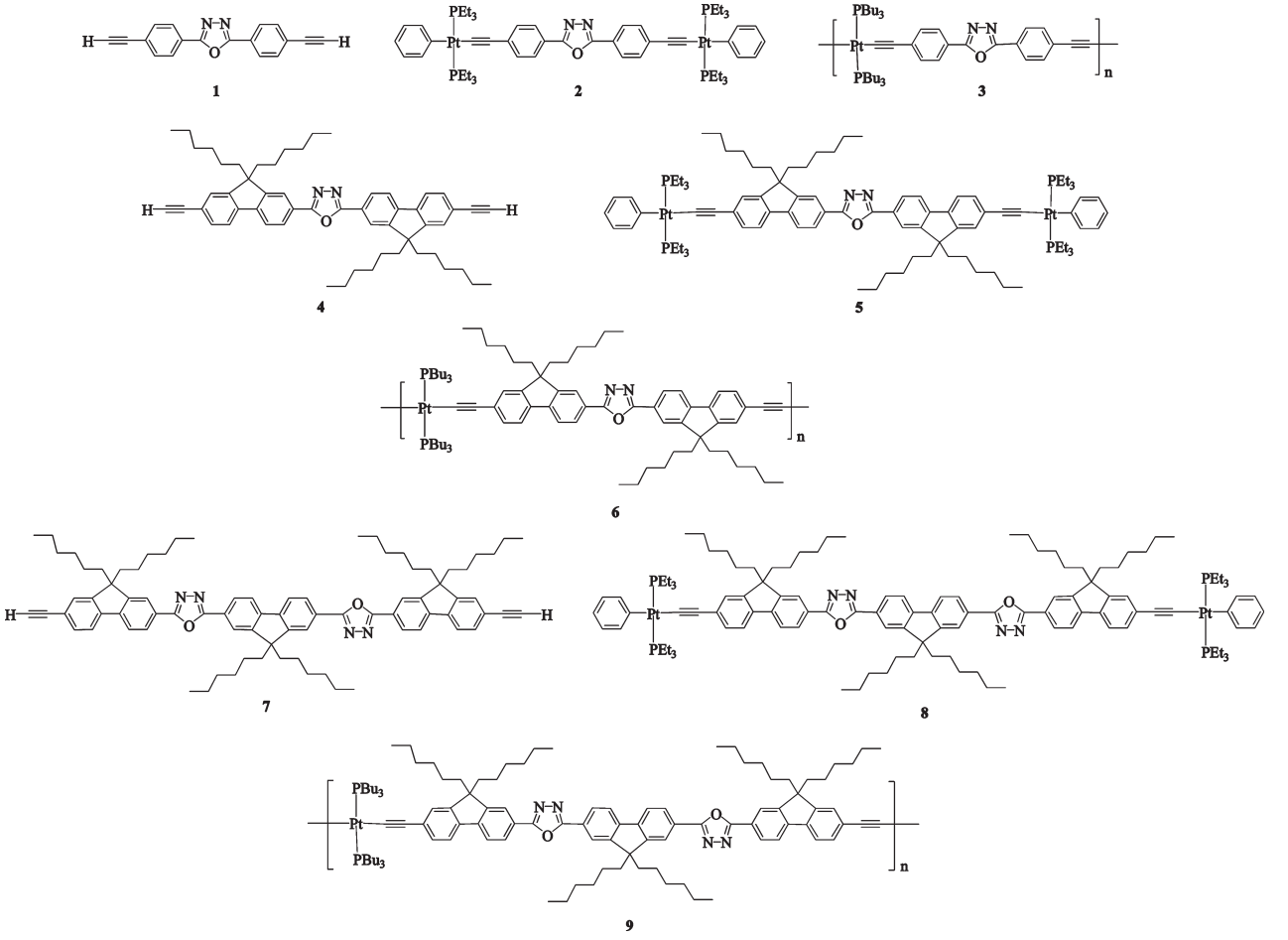

also support the nature of the frontier molecular orbitals (MOs) as π and π^* localized, leading to the formation of low-lying $\pi\pi^*$ excited states. In addition, there is growing interest in developing two-photon absorption (2PA) organic chromophores, which can play an important role in 3D microfabrication, ultra-high-density optical data storage, optical-limiting devices, up-converted lasing, photodynamic therapy, and so on.[15] Along this line, conjugated ethynylene-linked (−C≡C−) systems are attractive candidates,[15a] and the electron-poor nature of the **Ox** ring causes it to show promise as an electron-acceptor in the design of new 2PA chromophores.[11a] Hence, the 2PA and electroluminescence properties of these Pt-containing materials have been investigated to probe their potential optoelectronic applications.

Experimental Section

General. All reactions were carried out under a nitrogen atmosphere with the use of standard Schlenk techniques, but no special precautions were taken to exclude oxygen during workup. Solvents were predried and distilled from appropriate drying agents. All reagents and chemicals, unless otherwise stated, were purchased from commercial sources and used without further purification. Preparative TLC was performed on 0.7 mm silica plates (Merck Kieselgel 60 GF_{254}) prepared in our laboratory. Solvents were predried and distilled from appropriate drying agents. The compounds 2,5-bis(ethynylphenyl)-1,3,4-oxadiazole (**1**),[11a,16] *trans*-$[PtCl(Ph)(PEt_3)_2]$,[17] and *trans*-$[PtCl_2(PBu_3)_2]$[18] were prepared by the literature methods.

Instruments. Infrared spectra were recorded as CH_2Cl_2 solutions using a Perkin-Elmer Paragon 1000 PC or Nicolet Magna 550 Series II FTIR spectrometer, using CaF_2 cells with a 0.5 mm path length. NMR spectra were measured in appropriate solvents on a Jeol EX270 or a Varian Inova 400 MHz FT-NMR spectrometer with ^1H and ^{13}C NMR chemical shifts quoted relative to $SiMe_4$ and ^{31}P chemical shifts quoted relative to an 85% H_3PO_4 external standard. Fast atom bombardment (FAB) mass spectra were recorded on a Finnigan MAT SSQ710 mass spectrometer. The molecular weights of the polymers were determined by gel permeation chromatography (GPC) on a HP 1050 series HPLC system with visible wavelength and fluorescence detectors using polystyrene standards, and thermal analyses were performed with Perkin-Elmer Pyris Diamond DSC and Perkin-Elmer TGA6 thermal analyzers. Electrochemical measurements were made using a Princeton Applied Research model 273A potentiostat. The cyclic voltammetry experiment of the polymer film was performed at a scan rate of 100 mV s^{-1} using a eDAQ EA161 potentiostat electrochemical interface equipped with a thin-film-coated ITO-covered glass working electrode, a platinum counter electrode, and a Ag/AgCl (in 3 M KCl) reference electrode. The solvent in all measurements was deoxygenated MeCN, and the supporting electrolyte was 0.1 M $[^nBu_4N][PF_6]$. Thin polymer films were deposited on the working electrode by dip-coating in chlorobenzene solution (6 mg mL^{-1}). The onset reduction potential ($E_{onset,\ red}$) and optical bandgap (E_g) were used to determine the HOMO and LUMO energy levels using the equations $E_{LUMO} = [-(E_{onset,red\ (vs\ Ag/AgCl)} - E_{onset(NHE\ vs\ Ag/AgCl)})] - 4.50$ eV and $E_{HOMO} = (E_{LUMO} - E_g)$ eV, where the potentials for NHE versus vacuum and NHE versus Ag/AgCl are 4.50 and −0.22 V, respectively.[19] The photophysical measurements were generally carried out in 2MeTHF, which was distilled over calcium hydride under argon. The UV−visible spectra were recorded on a Hewlett-Packard diode array model 8452A. The emission spectra were obtained using a double monochromator Fluorolog 2 instrument from Spex. The emission lifetimes were measured on a TimeMaster

model TM-3/2003 apparatus from Photon Technology International (PTI). The source was a high-resolution nitrogen dye laser (fwhm ~1400 ps), and the fluorescence lifetimes were obtained from deconvolution or distribution lifetimes analysis. The minimum fluorescence lifetime that could be confidently and reproducibly measured with this system is 100 ps (http://www.pti-nj.com/LaserStrobe/LaserStrobe.html). This accuracy was also previously checked on a picosecond laser system (fwhm: 35 ps) at the University of Ottawa.[20] The uncertainties were about 10−50 ps based on multiple measurements (3−5 trials). Some of the phosphorescence lifetimes were performed on a PTI LS-100 system using a 1 μs tungsten-flash lamp (fwhm ~1 μs). The transient absorption spectra and kinetic data were acquired on a flash photolysis system from Luzchem model mLFP-111. The white probe light source was an ozone-free ceramic xenon lamp (Cermax; 175 W) equipped with a 125 mm monochromator and a R7400U-20 Hamamatsu compact photomultiplier. A Tektronix 9-bit digitizer TDS-3000 series with 300 MHz bandwidth was used. The pump excitation was the 355 nm line of a YAG laser from Continuum (Surelite) and the 530 nm line from OPO module (SL OPO PLUS) pumped at 355 nm by the same laser (fwhm = 13 ns). Typically, the pulse energy was ~90 mJ per pulse for all experiments. Quantum yield measurements were performed in 2MeTHF at 77 and 298 K. For the 298 K measurements, the samples were prepared under an inert atmosphere (in a glovebox, P_{O_2} < 50 ppm), and the solutions were inserted in a 1 cm airtight cuvette. At 77 K, the solutions were inserted in a NMR tube of 0.4 cm diameter, which was inserted inside an EPR Dewar filled with liquid N_2. This tube was fixed so that it would not move during measurements and would retain an identical position when changing samples. For both temperatures, the sample and standard concentrations were both adjusted to obtain an absorbance of 0.050 at the excitation wavelength, and each absorbance value was measured 10 times for better accuracy. Such methodology gives a reproducibility of the absorbance measurements of ±0.003 to 0.004. The 10% uncertainty on the quantum yield was evaluated based on multiple measurements (at least 3 to 5) and represents the maximum fluctuation in the measurements. The reference used for emission quantum yield was 9,10-diphenylanthracene (Φ_F = 1.0).[21]

Computations. All calculations were performed on a super computer from the Université de Sherbrooke (Mammouth MP) and supported by the Réseau Québécois de Calcul de Haute Performance with the Gaussian 03 revision C.02 and Gausview 3.0 software package.[22] The time-dependent density functional theory (TDDFT)[23−25] and DFT[26−29] computations were performed using the B3LYP method[30−32] with the 6-31G(d) basis sets[33−38] on all C, N, and O atoms. Basis sets and specific core electron approximations on Pt[39] and P atoms[40] were used.

Syntheses. The syntheses of all the ligand precursors are given in the Supporting Information.

Syntheses of Platinum(II) Model Complexes. A typical procedure was given for **2**. To a stirred mixture of **1** (25.0 mg, 0.093 mmol) and *trans*-[PtCl(Ph)(PEt_3)$_2$] (101.0 mg, 0.185 mmol) in Et_3N (10 mL) and CH_2Cl_2 (10 mL) was added CuI (3.00 mg). The solution was stirred at room temperature over a period of 12 h, after which all volatile components were removed under vacuum. The crude product was taken up in CH_2Cl_2 and purified on preparative silica TLC plates with CH_2Cl_2/*n*-hexane (1:1, v/v) as solvent. The product **2** was obtained as a yellow solid (70.3 mg, 0.055 mmol, 59%). IR (CH_2Cl_2): ν(C≡C) 2095 cm^{-1}. ^{1}H NMR ($CDCl_3$, δ): 7.97−7.94 (m, 4H, Ar), 7.41−7.25 (m, 8H, Ar), 7.00−6.95 (m, 4H, Ar), 6.81 (m, 2H, Ar), 1.76 (m, 24H, alkyl), 1.11 (m, 36H, alkyl). ^{13}C NMR ($CDCl_3$, δ): 104.37, 155.64, 138.88, 132.80, 131.15, 127.25, 126.36, 121.28, 120.07, 119.53, 110.31 (Ar + C≡C), 15.18, 8.11 (alkyl). ^{31}P NMR ($CDCl_3$, δ): 11.02 ($^1J_{P-Pt}$ = 2629 Hz). FAB-MS: *m*/*z* 1284 (M^+). Anal. Calcd for $C_{54}H_{78}N_2OP_4Pt_2$: C, 50.46; H, 6.12; N, 2.18. Found: C, 50.68; H, 6.32; N, 2.28.

5: Off-white solid. Yield: 77%. IR (KBr): ν(C≡C) 2090 cm^{-1}. ^{1}H NMR ($CDCl_3$, δ): 8.16−8.10 (m, 4H, Ar), 7.77 (m, 2H, Ar), 7.61 (m, 2H, Ar), 7.39−7.31 (m, 8H, Ar), 7.01−6.97 (m, 4H, Ar), 6.85−6.81 (m, 2H, Ar), 2.09−1.96 (m, 8H, alkyl), 1.85−1.78 (m, 24H, alkyl), 1.18−1.01 (m, 60H, alkyl), 0.78−0.75 (m, 12H, alkyl), 0.73−0.60 (m, 8H, alkyl). ^{13}C NMR ($CDCl_3$, δ): 165.14, 156.14, 151.59, 151.12, 144.88, 139.06, 136.58, 130.04, 129.20, 127.31, 125.94, 125.38, 121.51, 121.28, 121.11, 119.85, 119.65, 115.20, 111.42 (Ar + C≡C), 55.11 (quat. C), 40.33, 31.49, 29.63, 23.66, 22.54, 15.03, 13.98, 8.05 (alkyl). ^{31}P NMR ($CDCl_3$, δ): 10.77 ppm ($^1J_{P-Pt}$ = 2632 Hz). FAB-MS: *m*/*z* 1798 (M^+). Anal. Calcd for $C_{92}H_{134}N_2OP_4Pt_2$: C, 61.45; H, 7.51; N, 1.56. Found: C, 61.65; H, 7.67; N, 1.86.

8: Yellow solid. Yield: 91%. IR (KBr): ν(C≡C) 2087 cm^{-1}. ^{1}H NMR ($CDCl_3$, δ): 8.22−8.12 (m, 8H, Ar), 7.95−7.73 (m, 2H, Ar), 7.78 (m, 2H, Ar), 7.62 (m, 2H, Ar), 7.40−7.31 (m, 8H, Ar), 7.00−6.97 (m, 4H, Ar), 6.84−6.81 (m, 2H, Ar), 2.21 (m, 12H, alkyl), 1.84−1.73 (m, 24H, alkyl), 1.17−0.99 (m, 72H, alkyl), 0.78−0.72 (m, 18H, alkyl), 0.67−0.63 (m, 12H, alkyl). ^{13}C NMR ($CDCl_3$, δ): 165.47, 164.75, 156.23, 156.12, 156.01, 152.28, 151.67, 151.39, 151.15, 145.10, 143.29, 139.08, 136.74, 136.51, 130.08, 129.33, 128.77, 127.83, 127.67, 127.34, 126.20, 125.41, 123.51, 121.39, 121.33, 121.20, 120.95, 120.17, 119.91, 119.72, 115.53, 115.39, 115.24, 111.43 (Ar + C≡C), 55.97, 55.15 (quat. C), 40.34, 40.28, 31.50, 29.65, 29.53, 23.79, 23.69, 22.56, 22.49, 15.06, 14.00, 13.95, 8.06 (alkyl). ^{31}P NMR ($CDCl_3$, δ): 10.77 (J_{P-Pt} = 2636 Hz). FAB-MS: *m*/*z* 2198 (M^+). Anal. Calcd for $C_{119}H_{166}N_4O_2P_4Pt_2$: C, 65.01; H, 7.61; N, 2.55. Found: C, 65.32; H, 7.70; N, 2.66.

Syntheses of Platinum(II) Polymers. A typical procedure was given for **3**. We carried out polymerization by mixing **1** (25.0 mg, 0.093 mmol), *trans*-[$PtCl_2(PBu_3)_2$] (62.0 mg, 0.093 mmol), and CuI (3.00 mg) in Et_3N/CH_2Cl_2 (30 mL, 1:1 v/v). After stirring at room temperature overnight, the solution mixture was evaporated to dryness. The residue was redissolved in CH_2Cl_2 and filtered through a short silica column using the same solvent to remove ionic impurties and catalyst residues. After removal of the solvent, the crude product was purified by precipitation in CH_2Cl_2 from methanol twice. Subsequent drying in vacuo gave a yellow thin film of **3** (67.0 mg, 77%). IR (CH_2Cl_2): ν(C≡C) 2095 cm^{-1}. ^{1}H NMR ($CDCl_3$, δ): 7.99 (m, 4H, Ar), 7.40 (m, 4H, Ar), 2.16 (m, 12H, alkyl), 1.64−1.48 (m, 24H, alkyl), 0.95 (m, 18H, alkyl). ^{31}P NMR ($CDCl_3$, δ): 4.45 ($^1J_{P-Pt}$ = 2333 Hz). Anal. Calcd for $(C_{42}H_{62}N_2OP_2Pt)_n$: C, 58.12; H, 7.20; N, 3.23. Found: C, 58.23; H, 7.35; N, 3.43. TGA (N_2): T_{dec} = 315 °C. GPC (THF): M_w = 35 650, M_n = 16 370, PDI = 2.18, DP = 19.

6: Yellow solid. Yield: 79%. IR (KBr): ν(C≡C) 2091 cm^{-1}. ^{1}H NMR ($CDCl_3$, δ): 8.12 (br, s, 4H, Ar), 7.78 (br, s, 2H, Ar), 7.63 (br, s, 2H, Ar), 7.30 (br, s, 4H, Ar), 2.08 (br, s, 20H, alkyl), 1.69 (br, s, 12H, alkyl), 1.51 (br, s, 12H, alkyl), 1.11−0.90 (m, 42H, alkyl), 0.77 (br, s, 12H, alkyl), 0.64 (br, s, 8H, alkyl). ^{31}P NMR ($CDCl_3$, δ): 4.04 ($^1J_{P-Pt}$ = 2344 Hz). Anal. Calcd for $(C_{80}H_{118}N_2OP_2Pt)_n$: C, 69.59; H, 8.61; N, 2.03. Found: C, 69.34; H, 8.66; N, 2.18. TGA (N_2): T_{dec} = 351 °C. GPC (THF): M_w = 35 180, M_n = 19 390, PDI = 1.81, DP = 14.

9: Yellow solid. Yield: 81%. IR (KBr): ν(C≡C) 2092 cm^{-1}. ^{1}H NMR ($CDCl_3$, δ): 8.21−8.14 (m, 8H, Ar), 7.95 (m, 2H, Ar), 7.81 (m, 2H, Ar), 7.64 (m, 2H, Ar), 7.50−7.32 (m, 4H, Ar), 2.21 (m, 24H, alkyl), 1.69−1.43 (m, 28H, alkyl), 1.13−0.99 (m, 56H, alkyl), 0.78−0.64 (m, 24H, alkyl). ^{13}C NMR ($CDCl_3$, δ):165.40, 164.80, 152.29, 151.64, 151.40, 151.18, 143.31, 129.96, 126.22, 125.21, 123.50, 121.40, 121.23, 120.97, 120.09 (Ar), 55.97, 55.48, 55.23, 55.27 (quat. C), 40.47, 40.30, 31.56, 31.50, 29.69, 29.55, 26.44, 26.27, 26.08, 24.54, 24.47, 24.40, 24.35, 24.28, 24.22, 23.97, 23.73, 22.59, 22.51, 22.19, 22.02, 21.86, 13.99, 13.96, 13.85 (alkyl). ^{31}P NMR ($CDCl_3$, δ): 4.10 ($^1J_{P-Pt}$ = 2354 Hz). Anal. Calcd for $(C_{107}H_{150}N_4O_2P_2Pt)_n$: C, 72.14; H, 8.49; N, 3.15. Found: C, 72.36; H, 8.59; N, 3.45. TGA (N_2): T_{dec} = 353 °C. GPC (THF): M_w = 33 000, M_n = 16 380, PDI = 2.01, DP = 9.

X-ray Crystallography. Colorless crystals of **2** suitable for X-ray diffraction experiment were grown by slow evaporation of its solution in a $CHCl_3$/hexane mixture at room temperature

Scheme 1. Synthetic Routes to Ligand Precursors 4−2Br and 7−2Br

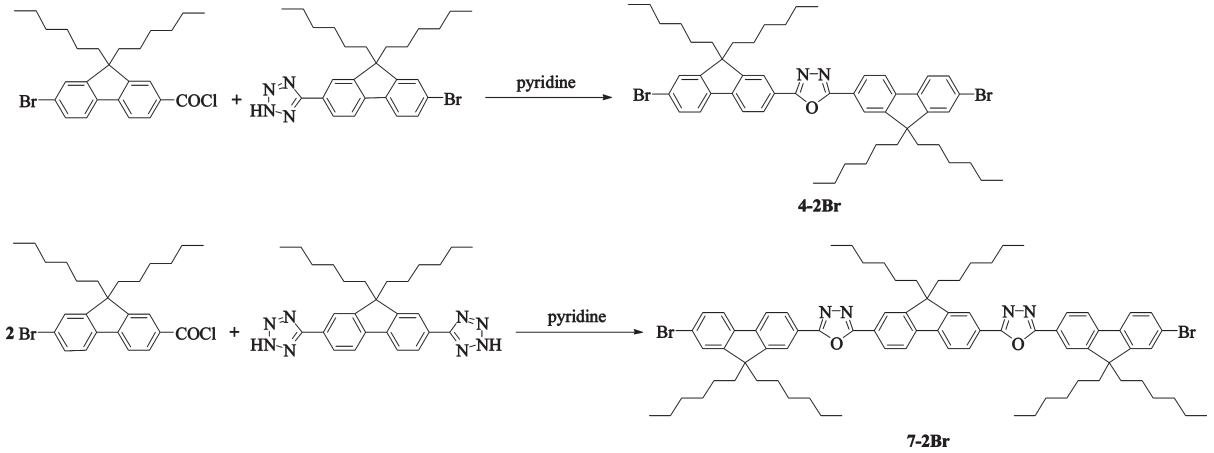

(r.t.). Geometric and intensity data were collected at 293 K using graphite-monochromated Mo Kα radiation (λ = 0.71073 Å) on a Bruker AXS Smart 1000 CCD area detector diffractometer. The collected frames were processed with the software SAINT,[41] and an absorption correction was applied (SADABS)[42] to the collected reflections. The structure was solved by the direct methods (SHELXTL)[43] in conjunction with standard difference Fourier techniques and subsequently refined by full-matrix least-squares analyses on F^2. All non-hydrogen atoms were assigned with anisotropic displacement parameters. Crystal data for **2**·C_6H_{14}: $C_{60}H_{92}N_2OP_4Pt_2$, M = 1371.42, monoclinic, space group $P\bar{1}$, a = 9.3231(5), b = 15.7367(8), c = 22.376(1) Å, α = 86.688(1), β = 88.983(1), γ = 81.850(1)°, U = 3244.1(3) Å^3, Z = 2, T = 293 K, μ(Mo Kα) = 4.442 mm^{-1}, 16 157 reflections measured, 11 178 unique, R_{int} = 0.0270, final R_1 = 0.0362, wR_2 = 0.0928 for 8629 [$I > 2\sigma(I)$] observed reflections.

Two-Photon Absorption Measurements. For two-photon absorption experiments, the laser system comprised a Ti/sapphire femtosecond oscillator (Micra, Coherent, tuning range only covers 750−850 nm) and a Ti/sapphire femtosecond regenerative amplifier (Legend, Coherent, output beam ~150 fs duration, and 1 kHz repetition rate). The pulses from the Ti/sapphire amplifier were first down-converted with an optical parametric amplifier (TOPAS-C, Coherent) and then frequency-doubled by a BBO crystal to generate the 700 to 900 nm two-photon excitation (TPE) wavelengths. The lasers were focused to spot size ~50 μm via an f = 10 cm lens onto the sample. The emitting light was collected with a backscattering configuration into a 0.5 m spectrograph and detected by a liquid nitrogen-cooled CCD detector. A power meter was used to monitor the uniform excitation. The theoretical framework and experimental protocol for the two-photon absorption cross-section (σ_2) measurements have been outlined by Webb and Xu.[44] In this approach, the TPE ratios of the reference and sample systems are given by

$$\frac{\sigma_2^S \cdot \Phi^S}{\sigma_2^R \cdot \Phi^R} = \frac{C_R \cdot n_S \cdot F^S(\lambda)}{C_S \cdot n_R \cdot F^R(\lambda)}$$

where Φ is the quantum yield, C is the concentration, n is the refractive index, and $F(\lambda)$ is the integrated photoluminescence spectrum. In our measurements, we ensured that the excitation flux and the excitation wavelengths were the same for both the sample and the reference. The σ_2 values of our compounds were determined using Rhodamine 6G as a reference.[45]

Results and Discussion

Synthesis and Chemical Characterization. Literature procedures[46] indicate that oxadiazole compounds can be prepared from the reaction of carboxylic chloride precursors with the corresponding tetrazole compounds. The synthetic approach used in this part started with 2,7-dibromofluorene. The carbonitrile derivatives (viz. 2-bromo-7-cyano-9,9-dihexylfluorene and 2,7-dicyano-9,9-dihexylfluorene) were prepared from 2,7-dibromo-9,9-dihexylfluorene. (See the Supporting Information.) Even when 1 equiv of CuCN was used, the disubstituted compounds had been produced. Fortunately, the separation of the monosubstituted product from the disubstituted product was easily achieved by column chromatography. 2-Bromo-7-tetrazolyl-9,9-dihexylfluorene and 2,7-bis(tetrazolyl)-9,9-dihexylfluorene were prepared from the corresponding carbonitrile derivatives through reaction with NaN_3 and NH_4Cl. By reacting 2-bromo-7-formyl-9,9-dihexylfluorene with $KMnO_4$, it was converted to the corresponding carboxylic acid, which further reacts with thionyl chloride under reflux to give the acid chloride.

Following the steps presented in Scheme 1, reaction of 2-bromo-7-chlorocarbonyl-9,9-dihexylfluorene with 2-bromo-7-tetrazolyl-9,9-dihexylfluorene affords **4−2Br**, whereas the former species reacts with 2,7-bis(tetrazolyl)-9,9-dihexylfluorene to produce **7−2Br**. Such reaction for species with two tetrazole groups is more difficult than the reaction involving one tetrazole group, so the yield of **7−2Br** was lower than that of **4−2Br**. The trimethylsilyl (TMS) acetylenic compounds were then prepared from the palladium-catalyzed Sonogashira coupling reaction sequence from **4−2Br** and **7−2Br**, and they were then converted into the diethynyl organic precursors **4** and **7** in moderate yields following the proto-desilylation approach using K_2CO_3 in MeOH as the base (Scheme 2).[47] In both **4** and **7**, the **Ox** units are evenly dispersed in the main chain at every one (for **4**) and three (for **7**) fluorene units.

Schemes 3 and 4 depict the synthesis of the model dinuclear Pt(II) complexes (**2**, **5**, **8**) and their corresponding metallopolymers (**3**, **6**, and **9**). Metal alkynylation reactions proceed via the CuI-catalyzed dehydrohalogenation synthetic protocol in the presence of an amine.[48] The desired Pt(II) diynes were isolated by preparative TLC plates on silica. For the polymers, isolation was accomplished by filtering the crude sample through a short column of silica gel using pure CH_2Cl_2 as the eluting solvent. Further purification can be made by precipitating the polymer solution in CH_2Cl_2 from MeOH to get high purity products..

All of the new metal complexes and polymers synthesized are air-stable and exhibit good solubility in common solvents such as CH_2Cl_2 and $CHCl_3$. GPC analysis was used to estimate the molecular weight of each polymer (Experimental Section) using polystyrene calibration. However, the data should be viewed

Scheme 2. Synthetic Pathways to Diethynyl Ligands 4 and 7

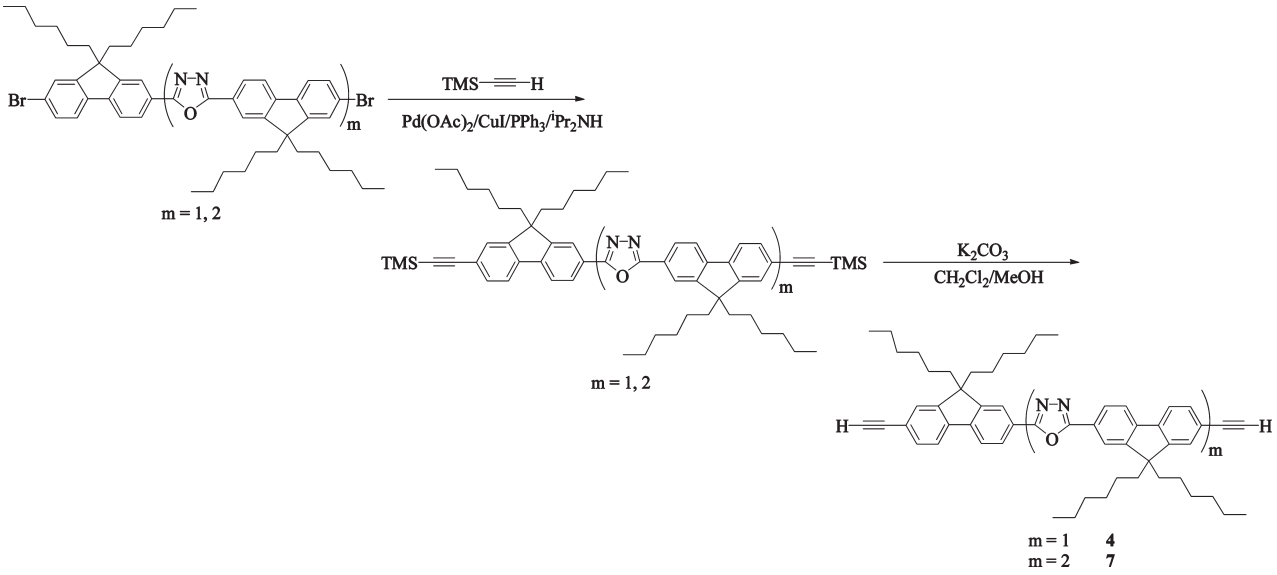

Scheme 3. Synthetic Pathway to Dinuclear Pt(II) Complexes 2, 5, and 8

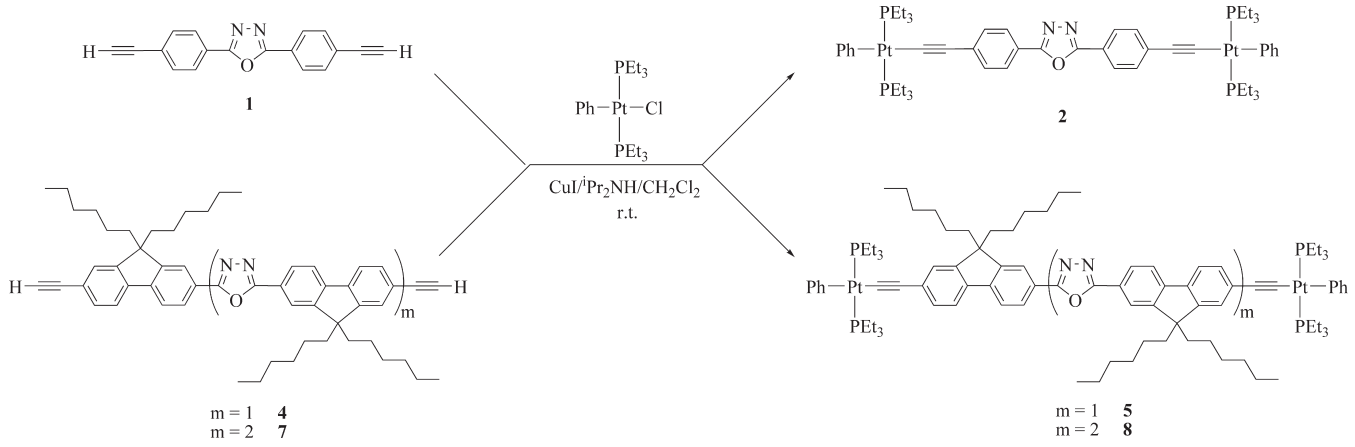

Scheme 4. Synthetic Pathway to Pt(II) Polyynes 3, 6, and 9

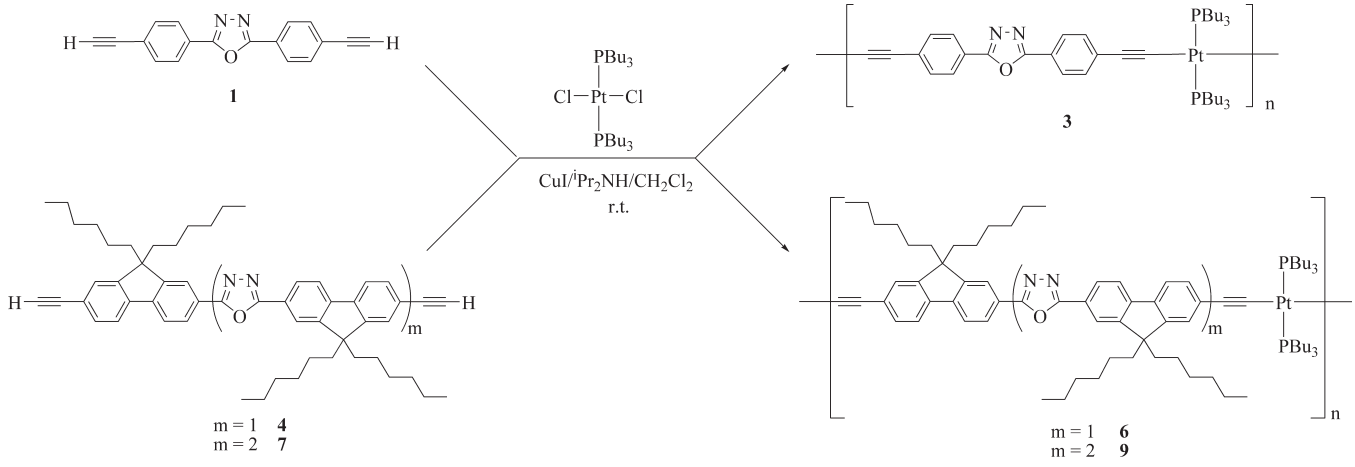

with caution in view of the common hurdles associated with utilizing GPC for rigid-rod polymers that would have appreciable differences in the hydrodynamic behavior from those for flexible polystyrene polymers. The number-average molecular weights (M_n) of these polymers range from 16 370 to 19 390 with a polydispersity index (M_w/M_n) between 1.81 and 2.18 and a degree of polymerization (DP) of ~19, 14, and 9 for **3**, **6**, and **9**, respectively (corresponding to ~57, 42, and 45 aromatic rings in total). The thermal properties of polymers were examined by thermal gravimetric analysis (TGA) and differential scanning calorimetry (DSC) under nitrogen. Analysis of the TGA trace (heating rate of 20 °C min^{-1}) for the polymers shows that they

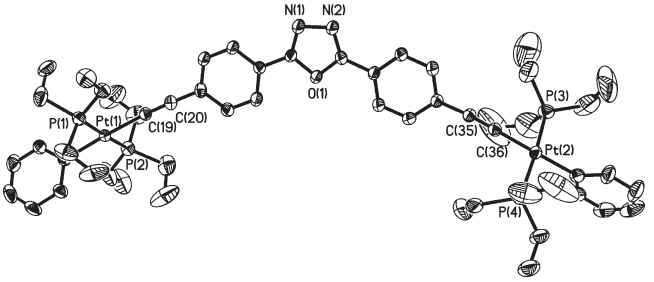

Figure 1. Perspective drawing of the structure of **2**; hydrogen atoms are omitted for clarity. Thermal ellipsoids were shown at the 25% probability levels. Selected bond lengths (angstroms) and angles (degrees): Pt(1)−P(1) 2.293(1), Pt(1)−P(2) 2.286(1), Pt(2)−P(3) 2.288(1), Pt(2)−P(4) 2.286(1), Pt(1)−C(19) 2.011(4), Pt(2)−C(36) 1.996(4), C(19)−C(20) 1.196(5), C(35)−C(36) 1.217(5); Pt(1)−C(19)−C(20) 175.9(4), and Pt(2)−C(36)−C(35) 176.2(4).

have excellent thermal stability with onset decomposition temperatures (T_{dec}) above 350 °C for **6** and **9**. Their degradation patterns are quite similar, which are ascribed to the elimination of PBu_3 and butyl groups from the polymers. In DSC studies, no phase transition signals are detected during repeated heating/cooling DSC cycles for both polymers. This observation probably results from the stiffness of the polymer chains.

Systematic characterization of these new compounds was achieved by analytical and spectroscopic methods. The solution IR spectra of these new metal complexes display a single sharp ν(C≡C) absorption band in the range of 2087−2095 cm^{-1}, revealing a trans configuration of the ethynylene ligands around the Pt center. The NMR spectral data revealed that these compounds have well-defined and symmetrical structures. ^{31}P NMR spectra of the Pt(II) complexes exhibit a single resonance with a pair of Pt satellites confirming the trans arrangement of the phosphine ligands around platinum. The $^1J_{P-Pt}$ values in the Pt compounds (ca. 2629−2636 Hz for dimers; 2333−2354 Hz for polymers) are typical of those found for related *trans*-PtP_2 systems.[48] The formulas of the model complexes were successfully confirmed from the intense molecular ion peaks in the positive FAB mass spectra. The exact 3D solid-state structure of **2** has been established by a single-crystal X-ray analysis (Figure 1). The coordination geometry at each Pt center is square-planar with the two PEt_3 groups trans to each other, and both metal end groups are bridged by a 2,5-bis(ethynylphenyl)-1,3,4-oxadiazole unit. To our knowledge, this is the first structurally characterized example of the oxadiazole-linked Pt alkynyl complex. The two phenyl rings are essentially coplanar with the central **Ox** group (mean deviation ~2.3−4.7°), analogous to those found for some coordination polymers.[10a]

UV−vis and Emission Spectra. The optical absorption and emission spectra for our compounds in 2MeTHF at 298 and 77 K are presented in Figures 2−4. Metal-free compound **1** exhibits a broad absorption in the 250−350 nm window at 298 K. Upon cooling to 77 K, the photoluminescence (PL) spectrum exhibits vibronic features. At both temperatures, fluorescence is observed. This assignment is based on the close proximity of the fluorescence and absorption bands and the short emission lifetimes (< 1 ns; Tables 1 and 2). The fluorescence band shows vibronic features, again more pronounced at 77 K. No emission attributable to phosphorescence is detected for **1**. Compound **2** exhibits broad absorption features between 300 and 400 nm, representing a shift of ~50 nm from **1**. This shift is caused by the presence of extended conjugation with the two $Pt(PEt_3)_2Ph$ fragments. Fluorescence is also observed for **2** at both temperatures (298 and 77 K) along with vibronically structured

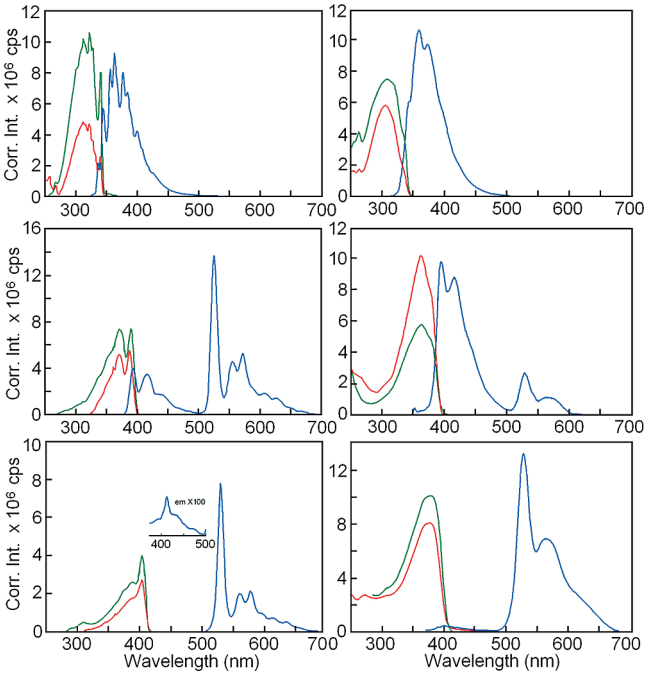

Figure 2. Absorption (red), excitation (green), and emission spectra (blue) of **1** (top), **2** (middle), and **3** (bottom) in 2MeTHF at 77 (left) and 298 K (right). At 77 K, the baseline of the absorption spectra deviates from linearity, and so the perfect correspondence between the excitation and absorption is not possible with a Dewar assembly.

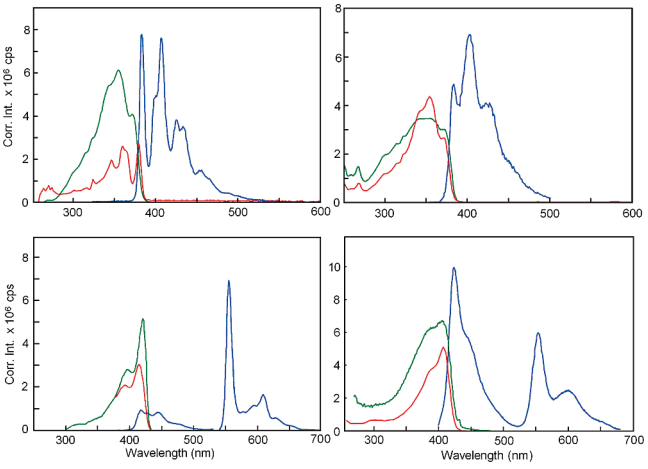

Figure 3. Absorption (red), excitation (green) and emission spectra (blue) of **4** (top) and **6** (bottom) in 2MeTHF at 77 (left) and 298 K (right). At 77 K, the baseline of the absorption spectra deviates from linearity, and so the perfect correspondence between the excitation and absorption is not possible with a Dewar assembly.

phosphorescence located at 525 nm for the 0−0 peak. The phosphorescence is easily assigned on the basis of the large gap between the absorption (390 nm) and emission (525 nm) and the long lifetimes in the μs time scale (Tables 1 and 2). Such assignment can also be rationalized in terms of the observed temperature dependence of the emission data for **2** and **3** (Figure 5). For **2**, the triplet PL band shows a strong temperature dependence in contrast with the higher-lying singlet emission. From 298 to 11 K, the singlet emission peak intensity increases only by a factor of 2.5, but the intensity of the corresponding lower-lying emission increases by a factor of 23.0; such an increase in emission intensity indicates a long-lived excited state that is more sensitive to thermally

activated nonradiative decay mechanisms.[49] The presence of triplet emission, in comparison with **1**, is due to the presence of heavy atom effect induced by the Pt center. For polymer **3**, the absorption band is red-shifted (by ~14 nm at 77 K from **2**), again due to extended conjugation, along with a weak fluorescence (shifted by ~5 nm) and very intense phosphorescence (relative to the fluorescence). The large change in relative intensity between the fluorescence and phosphorescence can also be attributed to heavy atom effect, but the increase in this effect may be due to the presence of conjugation, where the Pt may induce this effect upon a longer distance on the chain. The T_1 state appears strongly localized, as shown from the small energy difference between triplet emissions in the respective dimers and in the polymers. In all cases, the excitation spectra superimpose the absorption spectra. Time-resolved spectroscopy on the nanosecond and picosecond time scale was also employed to verify whether other weaker luminescence features were present under these bands, but none were found. Whereas no attempt was made to measure the photophysical data of **5** in detail here, the absorption, fluorescence, phosphorescence, and excitation spectra for the two other series, compound **4** and polymer **6**, as well as compounds **7** and **8** along with polymer **9**, behave the same way as described above for **1**−**3**. No further description is needed for these materials.

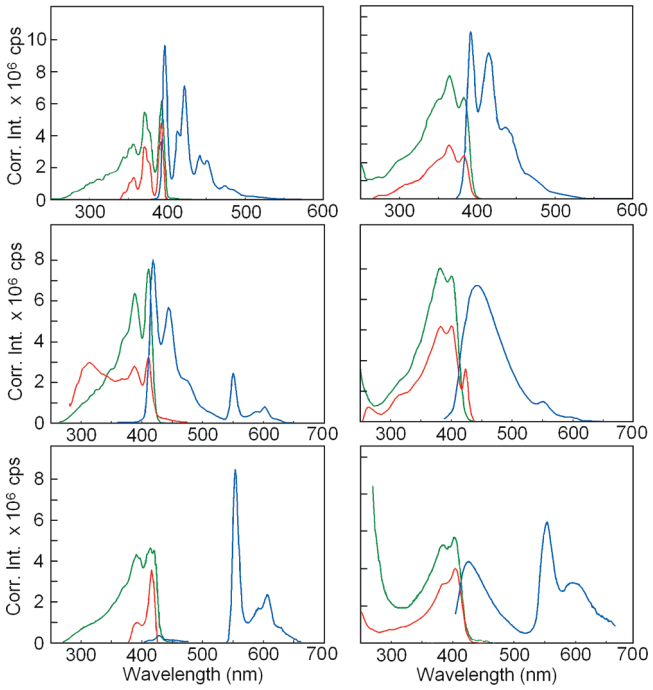

Figure 4. Absorption (red), excitation (green), and emission spectra (blue) of **7** (top), **8** (middle), and **9** (bottom) in 2MeTHF at 77 (left) and 298 K (right). At 77 K, the baseline of the absorption spectra deviates from linearity, and so the perfect correspondence between the excitation and absorption is not possible with a Dewar assembly.

The S_1-T_1 energy gaps for our Pt compounds are found to lie within the constant range of 0.7 ± 0.1 eV for similar conjugated metal polyynes.[50] The gap also compares well with the 0.6 to 0.7 eV estimated by Beljonne for an infinite PPV chain.[51] We attribute such a constant S_1-T_1 energy gap to the exchange energy and possibly some additional constant contribution due to the admixture of the Pt d orbitals.[52]

The fluorescence (τ_F, Φ_F) and phosphorescence (τ_P, Φ_P) lifetimes and quantum yields are reported in Tables 1 and 2. Both the lifetimes and quantum yields follow the trends: **1** > **2** > **3**, **4** > **6**, and **7** > **8** > **9**, apart from two exceptions. First, this trend is easily explained by the heavy atom effect induced by the Pt and by the increase in nonradiative internal conversion rate constants, k_{ic} (from the singlet) and k_{ip} (from the triplet), induced by the increase in molecular size (i.e., discrete molecule versus polymer).[50,53] The exceptions are for τ_F in **7** at 77 K and for τ_P in **8** at 298 K. Larger values (> 0.81 ns and 40 μs, respectively) were anticipated based on the trends. No explanation is available at this moment. One could also anticipate that the relative change in τ_F and Φ_F along the same trend should be very similar, but the decrease in Φ_F is larger than that of the τ_F. This is explained by the fact that the nature of molecules is changing and so the rate constant for fluorescence (k_F) is anticipated to change as well.

Table 1. UV−Vis Absorption and Emission Data at 77 K in 2MeTHF

	absorption λ (nm)	fluorescence λ (nm)	phosphorescence λ (nm)	τ_F (ns)	τ_P (μs)
1	312, 322, 340	345, 363, 377, 401	[a]	0.45 ± 0.03	[a]
2	372, 385	395, 418	525, 557, 573	0.31 ± 0.03	341 ± 4
3	404	413	530, 563, 580	0.10 ± 0.02	177 ± 3
4	380, 360	383, 407, 426, 457	[a]	0.45 ± 0.01	[a]
5	[b]	423, 449	551, 604	[b]	[b]
6	394, 416	419, 447	555, 610	0.16 ± 0.02	381 ± 1
7	358, 372, 392	397, 422, 442, 476	[a]	0.32 ± 0.03	[a]
8	388, 412	419, 445	551, 604	0.81 ± 0.03	669 ± 5
9	392, 416	424	553, 606	0.54 ± 0.02	396 ± 1

[a]Not observed. [b]Not measured.

Table 2. UV−Vis Absorption and Emission Data at 298 K in 2MeTHF

	absorption λ(nm)	fluorescence λ (nm)	Φ_F[b]	phosphorescence λ (nm)	Φ_P[b]	τ_F (ns)	τ_P (μs)	τ_{trans} (μs)[d]
1	306	361, 374	0.90	[a]	[a]	0.93 ± 0.04	[a]	[a]
2	364	395, 415	[c]	527, 566	[c]	0.39 ± 0.01	21 ± 2	18
3	378	403	0.003	529, 567	0.047	0.14 ± 0.03	19 ± 2	39
4	354	384, 404, 427	0.95	[a]	[a]	0.55 ± 0.09	[a]	320
5	383, 399	436	[c]	551, 604	[c]	[c]	[c]	[c]
6	408	425	0.013	555, 602	0.025	0.14 ± 0.03	3.3 ± 0.1	49
7	366, 384	392, 414, 434	0.96	[a]	[a]	0.90 ± 0.10	[a]	212
8	382, 402, 424	445	0.26	554	0.086	0.55 ± 0.02	10 ± 1	16
9	406	390, 427	0.013	555, 599	0.080	0.24 ± 0.03	39 ± 9	33

[a]Not observed. [b]Uncertainties are ±10%. [c]Not measured. [d]Uncertainties are large and hard to determine because of the large noise in the spectra. (See Figures 8 and 9.)

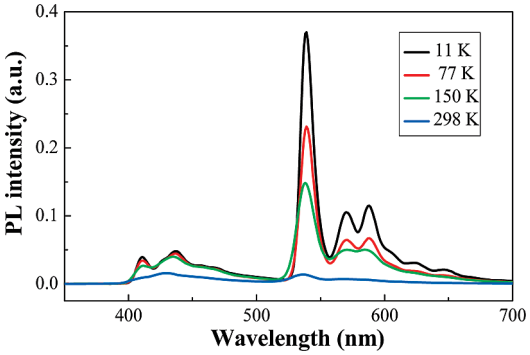

Figure 5. Temperature dependence of the PL spectra of **2**.

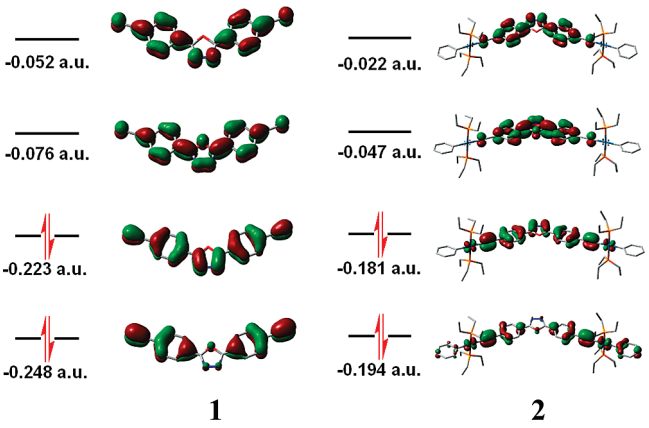

Figure 6. Frontier MOs of **1** and **2**.

Theoretical MO Treatments. The nature of the excited states for the studied molecules was addressed by DFT, and representations of the frontier MOs for **1** and **2** are given in Figure 6. The MOs for **1** are composed of π orbitals located on the ethynyl, benzene, and oxadiazole units, and $\pi\pi^*$ excited states are readily anticipated. For **2**, the HOMO-1, HOMO, LUMO, and LUMO+1 resemble that of **1**, except that in **2**, additional minor atomic contributions from the Pt atoms are also computed. For HOMO-1, some atomic contributions from the phenyl group are also observed. Moreover, the atomic contributions from the Pt atoms in the LUMO and LUMO+1 are very small. For **2**, $\pi\pi^*$ excited states are also expected, but a minor metal-to-ligand charge transfer (MLCT) character is also predicted where the ligand contribution is composed of the ethynyl, benzene, and oxadiazole units. No computation was performed for other compounds and polymers because of the structural similarity, and there is no doubt that a similar conclusion would be drawn. To check this, we also investigated compound **7** (Figure 7a).

The HOMO is predictably composed of the π-system of the three fluorene aromatics for **7**, with the two oxadiazole and ethynyl moieties having approximately equal atomic contributions. Therefore, the molecule is conjugated, consistent with the red shift of the lowest energy absorption band on going from compounds **1** (340) to **4** (380) to **7** (392 nm; 77 K). The HOMO-1 and HOMO-2 are also π-systems but differ in atomic contributions along the molecule, where little or almost no atomic contributions are computed for the middle fluorene and two oxadiazole rings (and the first ring of the outer fluorene), respectively. The LUMO, LUMO+1, and LUMO+2 are π-systems where the atomic distributions are weak on the outer and central fluorene moieties for the two former MOs, respectively, and more evenly distributed on the LUMO+2. The lowest energy electronic transitions and lowest energy excited states are predicted to be $\pi\pi^*$ in nature in all cases.

The absorption spectra of **1**, **2**, and **7** were calculated by TDDFT (Figure 7b) and were generated on the basis of the computed pure electronic transitions (0,0 components). The program computes the 30 first low-energy electronic transitions, providing a list of the predicted wavelengths (λ_{abs}) and oscillator strengths (f). Then, one assigns a thickness to each individual computed transition, and these bands are assembled together to generate a computed spectrum. Selected first individual calculated low-energy transitions are placed in Tables 3−5 for convenience, along with their major contributions. The positions of the lowest energy pure electronic transitions are 338.58, 382.49, and 411.55 nm for **1**, **2**, and **7**, respectively. These values compare favorably to the experimental values reported in Table 1 (340, 385, and 392 nm, respectively). Moreover, the relative intensity of the lowest energy absorption band with respect to the other ones placed on the blue side of the spectra is always the largest between 250 and 500 nm for both calculated and experimental spectra. In conclusion, the TDDFT study supports the conclusion of the MO analysis presented above.

Transient Absorption Spectra. The femtosecond transient absorption spectra of oxadiazole derivatives are known, and both S_1-S_n bands[54] and charge-separated states in oxadiazole-containing dyads[2a] have been investigated. Similarly, the transient T_1-T_n absorption spectra of oxadiazole derivatives are also known[55] and serve as a comparison for the investigated compounds and polymers. The nanosecond transient absorption spectra of model compound **2** and polymer **3** are characterized by two absorption bands at ~500 and 850 nm at 298 K (Figure 8). The spectra exhibit weak absorption, and consequently large uncertainties (maybe 30% in some measurements) are placed on the transient lifetimes. Nonetheless, except for polymer **6** (Figure 9), the lifetimes of the transient species and the phosphorescence lifetimes are very similar and indicate that these transient species are basically triplets. The T_1-T_n transient absorption spectra reported in the literature on the long time scale (nanosecond and microsecond) also exhibit a feature at 500−600 nm.[2a,55] All of this evidence clearly supports that the bands at 500 and 850 nm are T_1-T_n absorptions in **2** and **3**. The exception for the noncorrespondence in transient lifetime and phosphorescence lifetime for **6** is yet to be explained for the moment. Attempts to cool the samples to 77 K were made, but the presence of N_2 bubble in front of the probe light beams prevented acquisition of good quality data. In one case (compound **3**), the 77 K spectrum was obtained and resembled that of the 298 K spectrum (Figure 8). The red shifts of the two transient T_1-T_n absorption bands going from the ligand **4** to the polymer **6** reflect the increase in the extension of the conjugation.

Two-Photon Absorption Properties. Because the electron-deficient nature of **Ox** ring would foster its applications as an electron acceptor in the molecular design of 2PA chromophores, some of our complexes (**3**, **6**, and **9**) were selected for 2PA investigations. Figure 10 shows two-photon-induced excitation spectra of **3**, **6**, and **9** (λ_{em} = 505 nm for **3** and λ_{em} = 520 nm for **6** and **9**) and emission spectrum of **3** (λ_{ex} = 730 nm) in the DMSO solutions (1×10^{-4} M) by a femtosecond mode-locked Ti/sapphire laser. The two-photon-induced excitation and emission spectrum corresponds well with that obtained by linear single-photon excitation (Figure 2 and Table S1 in the Supporting Information). No linear absorption in the wavelength range of 500−800 nm was observed for these Pt(II) alkynyls, indicating that the

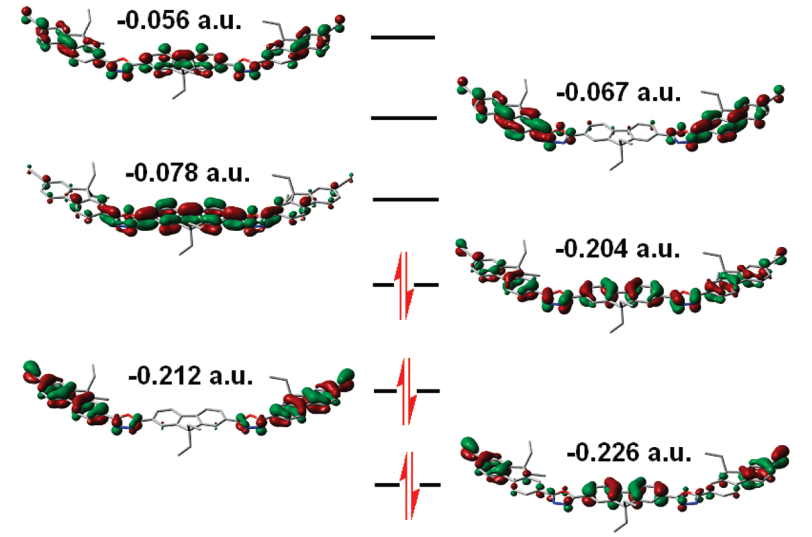

(a)

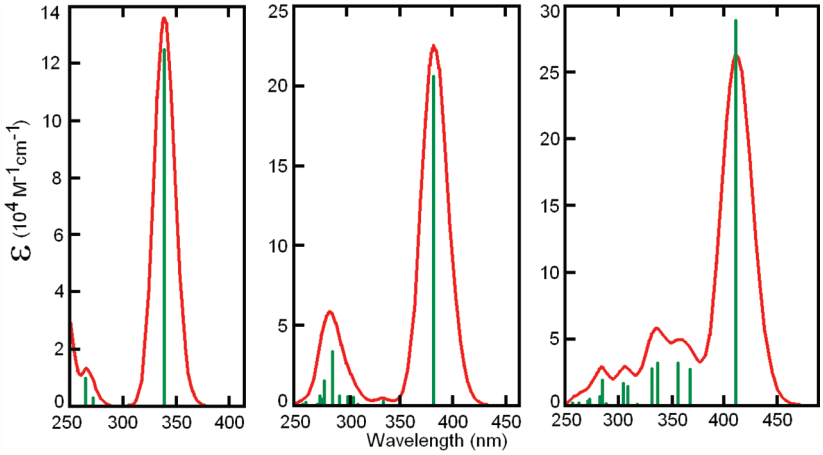

(b)

Figure 7. (a) Frontier MOs for **7**. (b) Computed absorption spectra by TDDFT for **1** (left), **2** (middle), and **7** (right).

Table 3. Computed Position of Selected Pure Electronic Transitions (0,0), Oscillator Strength (f), and Major Contributions for 1

entry	λ_{abs} (nm)	f	major contributions
1	338.58	1.249	HOMO → LUMO (0.66)
2	293.45	0.000	HOMO-1 → LUMO+1 (0.51), HOMO → LUMO+2 (0.48)
3	271.95	0.028	HOMO-2 → LUMO (0.51), HOMO-1 → LUMO (0.16), HOMO → LUMO+2 (0.38)

Table 4. Computed Position of Selected Pure Electronic Transitions (0,0), Oscillator Strength (f), and Major Contributions for 2

entry	λ_{abs} (nm)	f	major contributions
1	382.49	2.063	HOMO → LUMO (0.67)
2	338.70	0.000	HOMO-2 → LUMO (0.65), HOMO-2 → LUMO+1 (0.24)
3	338.10	0.000	HOMO-3 → LUMO (0.65), HOMO-3 → LUMO+1 (0.23)
4	334.43	0.035	HOMO-1 → LUMO+2 (0.65), HOMO → LUMO+2 (0.22)
5	310.43	0.009	HOMO-1 → LUMO+2 (0.31), HOMO → LUMO+1 (0.22), HOMO → LUMO+1 (0.56)

Table 5. Computed Position of Selected Pure Electronic Transitions (0,0), Oscillator Strength (f), and Major Contributions for 7

entry	λ_{abs} (nm)	f	major contributions
1	411.55	2.414	HOMO → LUMO (0.65), HOMO-1 → LUMO+1 (0.13)
2	368.39	0.229	HOMO-1 → LUMO (0.68)
3	356.18	0.268	HOMO → LUMO+1 (0.67)
4	336.74	0.268	HOMO-2 → LUMO (0.54), HOMO → LUMO+2 (0.32)
5	332.16	0.235	HOMO-1 → LUMO+1 (0.57), HOMO → LUMO+2 (0.36)

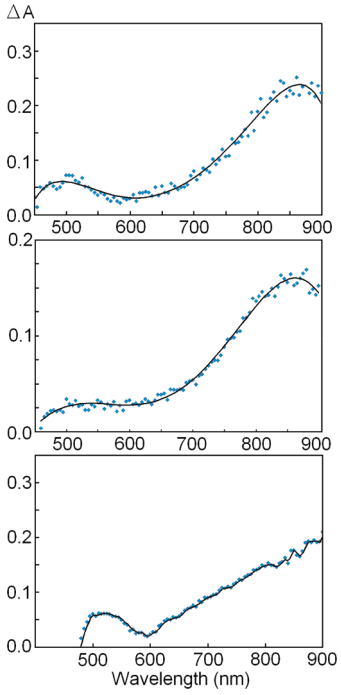

Figure 8. Transient absorption spectra of **2** (298 K, top) and **3** (298 K, middle; 77 K, bottom) in 2MeTHF. Delay time after the 355 nm laser pulse was 2 μs.

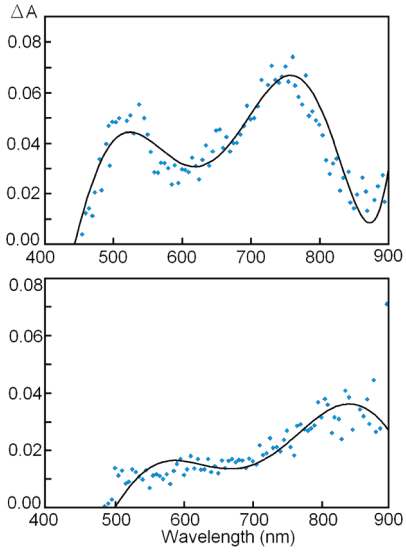

Figure 9. Transient absorption spectra of **4** (top) and **6** (bottom) in 2MeTHF at 298 K. Delay time after the 355 nm laser pulse was 2 μs.

emission induced by 730 nm excitation should not be attributed to a linear process but rather to a nonlinear event. The 2PA process at 730 nm was further confirmed by a power dependence experiment (inset of Figure 10b, with a slope of ~2.1).[56] The values of 2PA cross section (σ_2) of **3**, **6**, and **9** against Rhodamine 6G are 175, 280, and 260 GM (1 GM = 10^{-50} cm^4 s photon^{-1}), respectively, upon excitation at 730 nm. The σ_2 values for polymers **3**, **6**, and **9** are larger than those observed in *trans*-[Pt(PBu$_3$)$_2$(C≡C−C$_6$H$_4$−C≡C−C$_6$H$_5$)$_2$],[56,57] and some branched Pt(II) alkynyls recently reported[11a] and are also comparable to those for some small-molecular Pt−alkynylfluorene complexes.[58]

We also further investigated the two-photon induced photophysical properties of **7** to **9**. Comparing the σ_2 values for **7** to **9** (**7**: 130 GM, **8**: 330 GM, and **9**: 260 GM, λ_{ex} = 730 nm), it is clear that the values are found to be higher after metal coordination, but they do not differ much between Pt diyne and polyyne (i.e., **8** ≈ **9** > **7**). Incorporation of fluorene rings in **6** and **9** shows an enhancement effect on the σ_2 values relative to the nonfluorene species **3**. This observation is in line with that found in organic 2PA chromophores.[15] These findings have demonstrated that a hybrid of fluorene and oxadiazole moieties could serve as a promising building block for the construction of 2PA luminescence materials and the presence of Pt greatly enhances the sensitivity of 2PA for the materials.

Electrochemical and PLED Characterizations. Attention has been drawn to the development of conjugated polymers with improved electron-transporting capability.[59] Polymers with high electron affinities have lower barriers for electron injection from metal cathodes.[60] Polymers **3**, **6**, and **9** have a low-lying LUMO energy level (−3.83, −3.68, and −3.63 eV, respectively). These LUMO levels are lower than those of 2-(4-biphenylyl)-5-(4-*tert*-butylphenyl)-1,3,4-oxadiazole (PBD, −2.4 eV)[61] and other oxadiazole-based materials and that of poly(*p*-phenylenecyanovinylene) (−3.10 eV),[61] which demonstrates their good electron-transporting ability in PLEDs. The lower LUMO level of **3** than those of **6** and **9** is due to the lack of the more electron-rich fluorene groups in **3**. The HOMO energy levels of **3**, **6**, and **9** range from −6.82 to −6.52 eV, which makes them attractive candidates as the hole-blocking unit in PLEDs.

The polymeric nature of our Pt polyynes would simplify electrophosphorescent OLED characterization by the solution-processing techniques, so simple PLEDs based on **9** have been prepared by simple spin-coating method to yield thin polymer films with good morphological properties. The light-emitting polymer is better used as a phosphorescent dopant in a host rather than a neat emission layer in PLEDs to prevent the severe self-quenching and formation of aggregates expected in the solid film. PLEDs with the configuration of ITO/PEDOT−PSS (50 nm)/**9** (*x* wt %)−PVK−PBD (80 nm)/BCP (15 nm)/Alq$_3$ (30 nm)/LiF (1 nm)/Al (100 nm) (*x* = 1 and 5) were fabricated (ITO = indium tin oxide, PEDOT−PSS = poly(ethylenedioxythiophene)−poly(styrenesulfonic acid), PVK = poly(9-vinylcarbazole), BCP = 2,9-dimethyl-4,7-diphenyl-1,10-phenanthroline, Alq$_3$ = tris(8-hydroxyquinolinato)aluminum) and characterized as a function of applied voltage (Table 6). PVK functions as a host material that is electrically excited in PLEDs. For OLEDs/PLEDs, the charge transport properties of the host are important. It is desired that the host is bipolar in nature, however, for typical PVK, it is hole-dominated. Therefore, PBD is added to facilitate electron transport in the bulk. To improve the electroluminescence (EL) efficiency and to remove the electrical shorts between ITO and the luminescent layer, the PEDOT−PSS buffer layer was coated onto the ITO-coated glass substrate to boost hole injection and reduce current leakage. BCP acts as the hole-blocking layer and LiF (0.5 nm) acts as the electron injection layer. At higher voltages, emission from BCP becomes apparent in all cases because there are probably more holes than electrons, leading to the injection of holes into the BCP layer to result in its light emission upon electrical excitation. In each case, the low-energy EL peak resembles its PL phosphorescence spectrum from thin film, indicating that the same optical transition is responsible for light emission. Figure 11a shows the current density−voltage−luminance (*J*−*V*−*L*) curves of **9**-doped PLEDs at two doping concentrations. The luminance efficiency of the 1%-doped device as a function of current density is presented in Figure 11b. The best performance was realized at the maximum external quantum efficiency (η_{ext}) of 0.15%, a luminance efficiency (η_L) of 0.58 cd A^{-1}, and a power efficiency (η_p) of

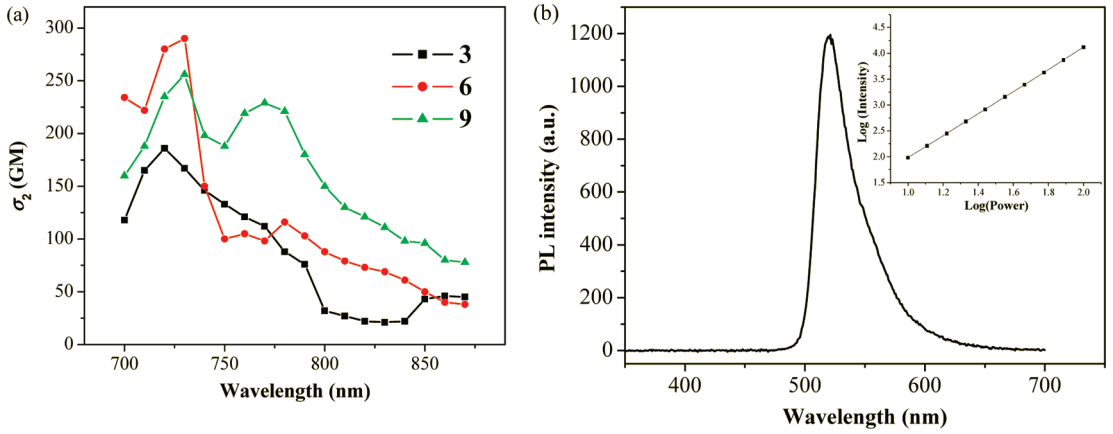

Figure 10. (a) Two-photon induced excitation spectra of **3**, **6**, and **9** (**3**: λ_{em} = 505 nm; **6** and **9**: λ_{em} = 520 nm) and (b) two-photon-induced emission spectrum of **3** (λ_{ex} = 730 nm) with the power dependence response curve in the inset.

Table 6. Performance of PLEDs Based on 9

phosphor dopant (wt %)	$V_{turn\text{-}on}$ [V]	luminance L [cd m^{-2}]	η_{ext} [%]	η_L [cd A^{-1}]	η_p [lm W^{1-}]	λ_{max} [nm][a]
1	10	480 (17.6)[b]	0.10[c] 0.15 (10.0)[b]	0.20[c] 0.58 (10.2)[b]	0.05[c] 0.16 (10.2)[b]	486, 555
5	11	439 (17.4)[b]	0.10[c] 0.11 (12)[b]	0.22[c] 0.24 (11.8)[b]	0.06[c] 0.07 (9.6)[b]	489, 555

[a]At 12 V. [b]Maximum values of the devices. Values in parentheses are the voltages at which they were obtained. [c]Values collected at 20 mA cm^{-2}.

0.16 lm W^{1-}. Each of the devices turned on at ~10−11 V for light emission at a luminance of 1 cd m^{-2}. The relatively high driving voltages relative to other typical vacuum-evaporated devices may be a result of the thicker emissive layer used and the large hole injection barrier from PEDOT−PSS to the HOMO of **9** at the PEDOT−PSS/**9** interface.[62] It is preferable to fabricate devices with a thicker emissive layer because a too-thin layer might lead to severe shorts or pinhole formation on the film that would reduce the device efficiency. For these devices, the EL spectra were dominated by two major emission bands, and a strong voltage dependence of the EL spectrum was observed. At high concentrations beyond 1 wt %, η_{ext} tends to decrease slightly, apparently because of less energy transfer from PVK to **9**; that is, concentration quenching effect occurred.[63]

Interestingly, to achieve the goal of white light emission, single-dopant white light electroluminescence (EL) with the simultaneous BCP fluorescence at ~485−490 nm[64] and polymer phosphorescence at ~555 nm has been realized as the voltage rises from 10 to 16 V (Figure 12a,b). For both devices, it was shown that upon increasing the bias voltage, the relative triplet−singlet intensity ratio of **9** decreases gradually at the expense of the orange vibronic-structured triplet emission, owing to the requirement for high energy excitation of BCP. Because polymer **9** has a lower HOMO level than those of PVK (−5.8 eV)[65] and PBD (−6.2 eV)[66] and even slightly lower than that of BCP (−6.1 eV),[67] the EL emission from BCP is gradually enhanced, and the BCP layer can sufficiently block the penetration of holes from PVK or PBD with increasing driving voltages. Accordingly, transport of holes through polymer **9** can occur to some extent; therefore, holes can be injected into the BCP layer to result in white EL emission in our devices. The highest achieved luminance is 440−480 cd m^{-2} at ~17 V, which is comparable to some white-light-emitting PLEDs derived from oxadiazole-containing organic polymers.[68,69] The CIE coordinates of these devices (Figure 12c) are fairly white and closely approach that of white light (defined as 0.33, 0.33). Upon increasing the concentration of **9**, it seems that the EL efficiencies are lowered gradually, but the relative BCP emission becomes more important in the EL spectra. This is consistent with more efficient intermolecular quenching of triplet excitons at high dopant concentrations.[1j] Whereas most examples of white

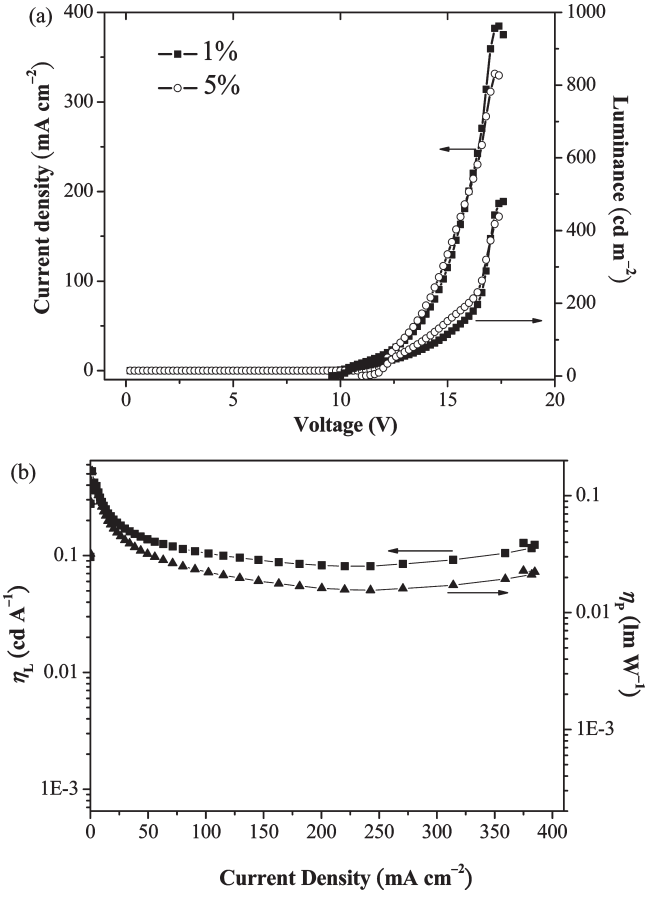

Figure 11. (a) Current density−voltage−luminance (J−V−L) characteristics of the PLED devices at two dopant concentrations of **9** and (b) EL efficiencies as a function of current density curve for the device at 1 wt % of dopant.

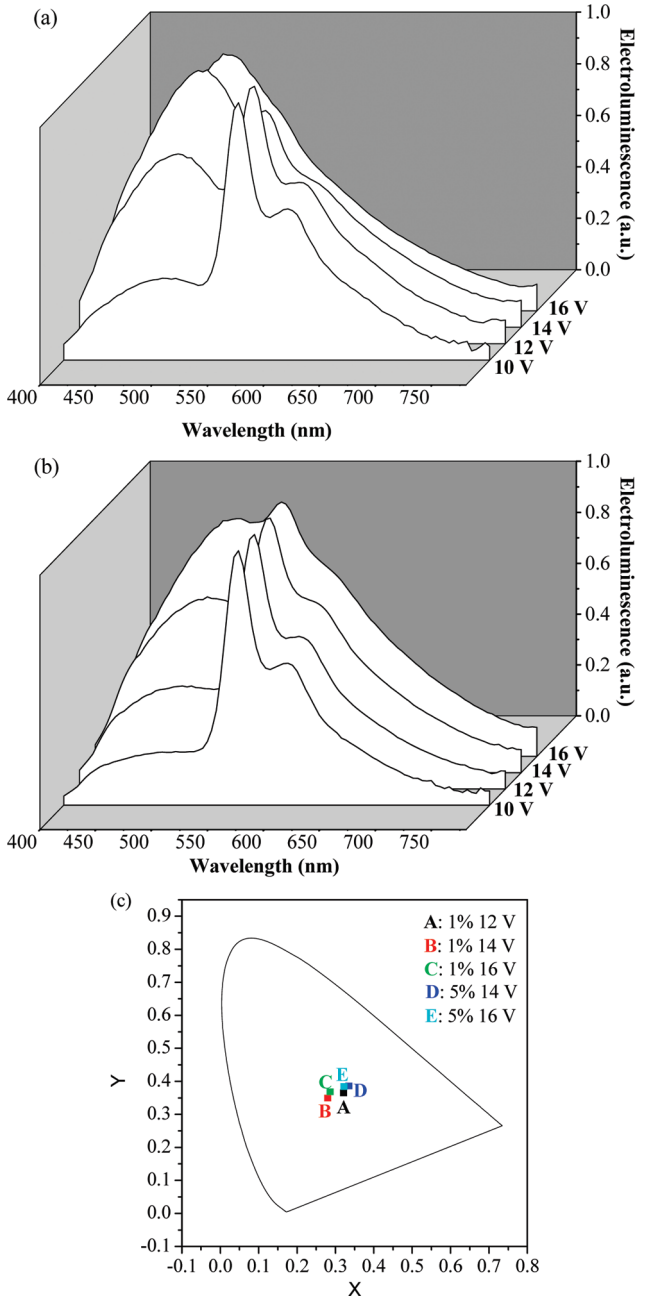

Figure 12. Electroluminescence spectra of PLED devices at different DC voltages applied (from front to back: 10, 12, 14, and 16 V) at (a) 1 wt % of **9** and (b) 5 wt % of **9**. (c) CIE coordinates of white light sources: A (0.321, 0.365); B (0.288, 0.349); C (0.286, 0.368); D (0.335, 0.386); and E (0.322, 0.384).

phosphorescent devices require dual or multiple dopants in multilayer devices, we note that a near-white EL has been achieved in this work using a single dopant configuration.

Conclusions

An original series of conjugated Pt-containing polyyne polymers using oxadiazole moiety along with their corresponding diplatinum model complexes were prepared and investigated for their photophysical properties. The results were compared with those for the compounds linked by the phenylene ring. The nature of the low-energy singlet and triplet excited states is $\pi\pi^*$ with some Pt d_{xy} orbital component, and geometry optimizations based on DFT calculations predict totally planar geometry, allowing better π-conjugation across the main chain. Because of this planarity, the **Ar-Ox-Ar** unit acts as a single chromophore, and no intrachain singlet and triplet energy or electron transfer was possible, as previously demonstrated in the 3,6- and 2,7-carbazole/fluorene-containing polymers we recently reported.[70] Consequently, the photophysical properties are bound to be different, as observed. For example, the addition of the **Ox** fragment would red shift the absorption and emission bands, leading to a tunable emission color in the resulting PLED devices. The presence of the Pt atom in the backbone enhances the phosphorescence emission. The 2PA cross sections (σ_2) of theses Pt-containing materials compare favorably to those of other reported small-molecule Pt alkynyl complexes. The design of electrophosphorescent PLED devices was made, and their uses as single-dopant white-light sources have also been described. Nearly white PLEDs were obtained under suitable operating conditions. Such results are interesting because examples of WPLED built on organometallic polymers of platinum are still relatively limited. This work illustrates that the use of Pt-containing organometallics in the design of WPLED is possible, which are prone to show promises for improvement. Moreover, because organo-transition-metal complexes can show much longer emission lifetimes than the purely organic compounds, the two-photon-induced longer-lived emitters should be of future interest for materials and polymer chemists and even also for biochemists for their further studies, for example, in time-resolved imaging.

Acknowledgment. This research was supported by the Natural Sciences and Engineering Research Council of Canada (NSERC), le Fonds Québécois de la Recherche sur la Nature et les Technologies (FQRNT), and the Centre d'Études des Matériaux Optiques et Photoniques de l'Université de Sherbrooke. W.-Y.W. acknowledges the support from a GRF grant from the Hong Kong Research Grants Council (grant no: HKBU 202709), a FRG grant from Hong Kong Baptist University (FRG2/08-09/111), and the Croucher Senior Research Fellowship from the Croucher Foundation. The work was also supported by State Administration of Foreign Experts Affairs International Partnership Program for Creative Research Teams, Chinese Academy of Sciences.

Supporting Information Available: Synthetic procedures and spectroscopic data for all ligand precursors, temperature dependence of the PL spectra of **3**, time-resolved emission spectra of **2**−**4** and **7**−**9**, as well as some linear optical data of Pt polyynes. This material is available free of charge via the Internet at http://pubs.acs.org.

References and Notes

(1) (a) Zhao, B.; Liu, D.; Peng, L.; Li, H.; Shen, P.; Xiang, N.; Liu, Y.; Tan, S. *Eur. Polym. J.* **2009**, *45*, 2079–2086. (b) Choi, J.; Lee, B.; Kim, J. H.; Lee, K. *Macromol. Res.* **2009**, *17*, 319–324. (c) Chen, R.-T.; Chen, S.-H.; Hsieh, B.-Y.; Chen, Y. *J. Polym. Sci., Part A: Polym. Chem.* **2009**, *47*, 2821–2834. (d) Park, J. J.; Park, T. J.; Jeon, W. S.; Kim, S. Y.; Lee, Y. K.; Jang, J.; Kwon, J. H. *Mol. Cryst. Liq. Cryst.* **2009**, *498*, 290–297. (e) Wang, H.; Ryu, J.-T.; Han, Y. S.; Kwon, Y. *Mol. Cryst. Liq. Cryst.* **2009**, *499*, 18–25. (f) Gong, X.; Yang, Y.; Xiao, S. *J. Phys. Chem. C* **2009**, *113*, 7398–7404. (g) Pickup, D. F.; Yi, H.; Kun, H.; Iraqi, A.; Stevenson, M.; Lidzey, D. G. *Thin Solid Films* **2009**, *517*, 2840–2844. (h) Yang, Q.; Jin, H.; Xu, Y.; Wang, P.; Liang, X.; Shen, Z.; Chen, X.; Zou, D.; Fan, X.; Zhou, Q. *Macromolecules* **2009**, *42*, 1037–1046. (i) Wong, W.-Y.; He, Z.; So, S.-K.; Tong, K.-L.; Lin, Z. *Organometallics* **2005**, *24*, 4079–4082. (j) He, Z.; Wong, W.-Y.; Yu, X.; Kwok, H.-S.; Lin, Z. *Inorg. Chem.* **2006**, *45*, 10922–10937.

(2) (a) de Miguel, M.; Ferrer, B.; Teruel, L.; Garcia, H.; Jin, Y.; Li, Y.; Ding, J. *J. Phys. Chem. C* **2009**, *113*, 8471–8477. (b) Wen, S.; Pei, J.; Zhou, Y.; Xue, L.; Xu, B.; Li, Y.; Tian, W. *J. Polym. Sci., Part A: Polym. Chem.* **2009**, *47*, 1003–1012. (c) Sommer, J. R.; Farley, R. T.; Graham, K. R.; Yang, Y.; Reynolds, J. R.; Xue, J.; Schanze, K. S. *Appl. Mater. Interfaces* **2009**, *1*, 274–278.

(3) Huebner, C. F.; Carroll, J. B.; Evanoff, D. D.; Ying, Y.; Stevenson, B. J.; Lawrence, J. R.; Houchins, J. M.; Foguth, A. L.; Sperry, J.; Foulger, S. H. *J. Mater. Chem.* **2008**, *18*, 4942–4948.

(4) Wang, X.; Guang, S.; Xu, H.; Su, X.; Yang, J.; Song, Y.; Lin, N.; Liu, X. *J. Mater. Chem.* **2008**, *18*, 4204–4209.
(5) Gomes, D.; Nunes, S. P. *J. Membr. Sci.* **2008**, *321*, 114–122.
(6) Kannan, M. B.; Gomes, D.; Dietzel, W.; Abetz, V. *Surf. Coat. Technol.* **2008**, *202*, 4598–4601.
(7) Ponce, M. L.; Gomes, D.; Nunes, S. P. *J. Membr. Sci.* **2008**, *319*, 14–22.
(8) (a) Adachi, C.; Tsutsui, T.; Saito, S. *Appl. Phys. Lett.* **1990**, *56*, 799–801. (b) Adachi, C.; Tsutsui, T.; Saito, S. *Appl. Phys. Lett.* **1990**, *57*, 513–531.
(9) (a) Utsuki, K.; Takano, S. *J. Electrochem. Soc.* **1992**, *139*, 3610–3615. (b) Kido, J.; Nagai, K.; Okamoto, Y.; Skotheim, T. *Chem. Lett.* **1991**, 1267–1270. (c) Ohmori, Y.; Uchida, M.; Morishima, C.; Fujii, A.; Yoshino, K. *Jpn. J. Appl. Phys.* **1993**, *32*, L1663–L1666. (d) Takada, N.; Tsutsui, T.; Saito, S. *Appl. Phys. Lett.* **1993**, *63*, 2032–2034. (e) Kido, J.; Hayase, H.; Hongawa, K.; Nagai, K.; Okuyama, K. *Appl. Phys. Lett.* **1994**, *65*, 2124–2126. (f) Era, M.; Morimoto, S.; Tsutsui, T.; Saito, S. *Appl. Phys. Lett.* **1994**, *65*, 676–678. (g) Era, M.; Tsutsui, T.; Saito, S. *Appl. Phys. Lett.* **1995**, *67*, 2436–2438. (h) Kraft, A. *Chem. Commun.* **1996**, 77–79. (i) Zhan, X.; Liu, Y.; Wu, X.; Wang, S.; Zhu, D. *Macromolecules* **2002**, *35*, 2529–2537.
(10) (a) Dong, Y.-B.; Zhang, Q.; Wang, L.; Ma, J.-P.; Huang, R.-Q.; Shen, D.-Z.; Chen, D.-Z. *Inorg. Chem.* **2005**, *44*, 6591–6608. (b) Atoub, N.; Mahmoudi, G.; Morsali, A. *Inorg. Chem. Commun.* **2007**, *10*, 166–169. (c) Wang, Y.-T.; Tang, G.-M.; Ma, W.-Y.; Wan, W.-Z. *Polyhedron* **2007**, *26*, 782–790. (d) Zhao, X.-X.; Ma, J.-P.; Dong, Y.-B.; Huang, R.-Q; Lai, T. *Cryst. Growth Des.* **2007**, *7*, 1058–1068. (e) Zhang, Z.-H.; Tian, Y.-L.; Guo, Y.-M. *Inorg. Chim. Acta* **2007**, *360*, 2783–2788. (f) Richardson, C.; Steel, P. J. *Inorg. Chem. Commun.* **2007**, *10*, 884–887. (g) Wang, Y.-T.; Tang, G.-M; Qiang, Z.-W. *Polyhedron* **2007**, *26*, 4542–4550. (h) Mahmoudi, G.; Morsali, A. *CrystEngComm* **2007**, *9*, 1062–1072. (i) Zhang, Z.-H.; Li, C.-P.; Tian, Y.-L.; Guo, Y.-M. *Inorg. Chem. Commun.* **2008**, *11*, 326–329. (j) Zhang, Q.; Ma, J.-P.; Wang, P.; Shi, Z.-Q.; Dong, Y.-B.; Huang, R.-Q. *Cryst. Growth Des.* **2008**, *8*, 2581–2587. (k) Fard-Jahromi, M. J. S.; Morsali, A.; Zeller, M. *J. Coord. Chem.* **2008**, *61*, 2227–2233. (l) Singh, M.; Butcher, R. J.; Singh, N. K. *Polyhedron* **2009**, *28*, 95–100. (m) Zhang, Z.-H.; Du, M. *CrystEngComm* **2008**, *10*, 1350–1357.
(11) (a) Chan, C. K. M.; Tao, C.-H.; Tam, H.-L.; Zhu, N.; Yam, V. W.-W.; Cheah, K.-W. *Inorg. Chem.* **2009**, *48*, 2855–2864. (b) Jura, M.; Koentjoro, O. F.; Raithby, P. R.; Sharp, E. L.; Wilson, P. J. *Mater. Res. Soc. Symp. Proc.* **2005**, *846*, 59–64.
(12) (a) Liu, J.; Lam, J. W. Y.; Tang, B. Z. *Chem. Rev.* **2009**, *109*, 5799–5867. (b) Lam, J. W. Y.; Tang, B. Z. *Acc. Chem. Res.* **2005**, *38*, 745–754.
(13) (a) Neher, D. *Macromol. Rapid Commun.* **2001**, *22*, 1365–1385. (b) Wong, W.-Y. *Coord. Chem. Rev.* **2005**, *249*, 971–997. (c) Setayesh, S.; Grimsdale, A. C.; Weil, T.; Enkelmann, V.; Müllen, K.; Meghdadi, F.; List, E. J. W.; Leising, G. *J. Am. Chem. Soc.* **2001**, *123*, 946–954. (d) Yu, W. L.; Pei, J.; Huang, W.; Heeger, A. J. *Adv. Mater.* **2000**, *12*, 828–831. (e) Wong, K. T.; Chien, Y. Y.; Chen, R. T.; Wang, C. F.; Lin, Y. T.; Chiang, H. H.; Hsieh, P. Y.; Wu, C. C.; Chou, C. H.; Su, Y. O. *J. Am. Chem. Soc.* **2002**, *124*, 11576–11577.
(14) (a) Scherf, U.; List, E. *J. Adv. Mater.* **2002**, *14*, 477–487. (b) Wu, W. L.; Pei, Y.; Cao, Y.; Huang, W.; Heeger, A. J. *Chem. Commun.* **1999**, 1837–1838. (c) Grice, A. W.; Bradley, D. D. C.; Bernius, M. T.; Inbasekaran, M.; Wu, W. W.; Woo, E. P. *Appl. Phys. Lett.* **1998**, *73*, 629–631. (d) Pschirer, N. G.; Bunz, U. H. F. *Macromolecules* **2000**, *33*, 3961–3963. (e) Janietz, S.; Bradley, D. D. C.; Grell, M.; Glebeler, C.; Inbasekaran, M.; Woo, E. P. *Appl. Phys. Lett.* **1998**, *73*, 2453–2455. (f) Marsitzky, D.; Vestberg, R.; Blainey, P.; Tang, B. T.; Hawke, C. J.; Carter, K. R. *J. Am. Chem. Soc.* **2001**, *123*, 6965–6972.
(15) (a) Pawlicki, M.; Collins, H. A.; Denning, R. G.; Anderson, H. L. *Angew. Chem., Int. Ed.* **2009**, *48*, 3244–3266. (b) Terenziani, F.; Katan, C.; Badaeva, E.; Tretiak, S.; Blanchard-Desce, M. *Adv. Mater.* **2008**, *20*, 1–38.
(16) Wong, W. Y.; Guo, Y. H. *J. Mol. Struct.* **2008**, *890*, 150–156.
(17) Chatt, J.; Shaw, B. L. *J. Chem. Soc.* **1959**, 4020–4033.
(18) Chatt, J.; Hayter, R. G. *J. Chem. Soc., Dalton Trans.* **1961**, 896–904.
(19) (a) Hou, J.; Tan, Z.; Yan, Y.; He, Y.; Yang, C.; Li, Y. *J. Am. Chem. Soc.* **2006**, *128*, 4911–4916. (b) van de Walle, C. G.; Neugebauer, J. *Nature* (*London*) **2003**, *423*, 626–628.
(20) (a) Mohtat, N.; Cozens, F. L.; Scaiano, J. C. *J. Phys. Chem. B* **1998**, *102*, 7557–7562. (b) Cosa, G.; Vinette, A. L.; McLean, J. R. N.; Scaiano, J. C. *Anal. Chem.* **2002**, *74*, 6163–6169.
(21) Eaton, D. F. *Pure Appl. Chem.* **1988**, *60*, 1107–1114.
(22) Frisch, M. J.; Trucks, G. W.; Schlegel, H. B.; Scuseria, G. E.; Robb, M. A.; Cheeseman, J. R.; Montgomery, J. A., Jr.; Vreven, J. T.; Kudin, K. N., Burant, J. C.; Millam, J. M.; Iyengar, S. S.; Tomasi, J.; Barone, V.; Mennucci, B., Cossi, M., Scalmani, G.; Rega, N.; Petersson, G. A.; Nakatsuji, H.; Hada, M.; Ehara, M.; Toyota, K.; Fukuda, R.; Hasegawa, J.; Ishida, M.; Nakajima, T.; Honda, Y.; Kitao, O.; Nakai, H.; Klene, M.; Li, X.; Knox, J. E.; Hratchian, H. P.; Cross, J. B.; Adamo, C.; Jaramillo, J.; Gomperts, R.; Stratmann, R. E.; Yazyev, O.; Austin, A. J.; Cammi, R.; Pomelli, C.; Ochterski, J. W.; Ayala, P. Y.; Morokuma, K.; Voth, G. A.; Salvador, P.; Dannenberg, J. J.; Zakrzewski, V. G.; Dapprich, S.; Daniels, A. D.; Strain, M. C.; Farkas, O.; Malick, D. K.; Rabuck, A. D.; Raghavachari, K.; Foresman, J. B.; Ortiz, J. V.; Cui, Q.; Baboul, A. G.; Clifford, S.; Cioslowski, J.; Stefanov, B. B.; Liu, G.; Liashenko, A.; Piskorz, P.; Komaromi, R. L.; Martin, I.; Fox, D. J.; Keith, T.; Al-Laham, M. A.; Peng, C. Y.; Nanayakkara, A.; Challacombe, M.; Gill, P. M. W.; Johnson, B.; Chen, W.; Wong, M. W.; Gonzalez, C.; Pople, J. A. *Gaussian 03*, revision C.02; Gaussian, Inc.: Wallingford, CT, 2004.
(23) Stratmann, R. E.; Scuseria, G. E.; Frisch, M. J. *J. Chem. Phys.* **1998**, *109*, 8218–8224.
(24) Bauernschmitt, R.; Ahlrichs, R. *Chem. Phys. Lett.* **1996**, *256*, 454–464.
(25) Casida, M. E.; Jamorski, C.; Casida, K. C.; Salahub, D. R. *J. Chem. Phys.* **1998**, *108*, 4439–4449.
(26) Hohenberg, P.; Kohn, W. *Phys. Rev.* **1964**, *136*, B864–B871.
(27) Kohn, W.; Sham, L. J. *Phys. Rev.* **1965**, *140*, A1133–A1138.
(28) *The Challenge of d and f Electrons*; Salahub, D. R., Zerner, M. C., Eds.; ACS Symposium Series; American Chemical Society: Washington, DC, 1989.
(29) Parr, R. G.; Yang, W. *Density-Functional Theory of Atoms and Molecules*; Oxford University Press: Oxford, U.K., 1989.
(30) Becke, A. D. *J. Chem. Phys.* **1993**, *98*, 5648–5652.
(31) Lee, C.; Yang, W.; Parr, R. G. *Phys. Rev. B* **1988**, *37*, 785–789.
(32) Miehlich, B.; Savin, A.; Stoll, H.; Preuss, H. *Chem. Phys. Lett.* **1989**, *157*, 200–206.
(33) Ditchfield, R.; Hehre, W. J.; Pople, J. A. *J. Chem. Phys.* **1971**, *54*, 724–728.
(34) Hehre, W. J.; Ditchfield, R.; Pople, J. A. *J. Chem. Phys.* **1972**, *56*, 2257–2261.
(35) Hariharan, P. C.; Pople, J. A. *Mol. Phys.* **1974**, *27*, 209–214.
(36) Gordon, M. S. *Chem. Phys. Lett.* **1980**, *76*, 163–168.
(37) Hariharan, P. C.; Pople, J. A. *Theor. Chim. Acta* **1973**, *28*, 213–222.
(38) Blaudeau, J.-P.; McGrath, M. P.; Curtiss, L. A.; Radom, L. *J. Chem. Phys.* **1997**, *107*, 5016–5021.
(39) (a) Binkley, J. S.; Pople, J. A.; Hehre, W. J. *J. Am. Chem. Soc.* **1980**, *102*, 939–947. (b) Stevens, W. J.; Basch, H.; Krauss, M. *J. Chem. Phys.* **1984**, *81*, 6026–6033. (c) Stevens, W. J.; Krauss, M.; Basch, H.; Jasien, P. G. *Can. J. Chem.* **1992**, *70*, 612–630. (d) Cundariand, T. R.; Stevens, W. J. *J. Chem. Phys.* **1993**, *98*, 5555–5565.
(40) (a) Labello, N. P.; Ferreira, A. M.; Kurtz, H. A. *J. Comput. Chem.* **2005**, *26*, 1464–1471. (b) Labello, N. P.; Ferreira, A. M.; Kurtz, H. A. *Int. J. Quantum Chem.* **2006**, *106*, 3140–3148.
(41) *SAINT+*, version 6.02a; Bruker, Analytical X-ray System, Inc.: Madison, WI, 1998.
(42) Sheldrick, G. M. *SADABS, Empirical Absorption Correction Program*; University of Göttingen: Germany, 1997.
(43) Sheldrick, G. M. *SHELXTL*, Reference Manual, version 5.1; Madison, WI, 1997.
(44) Xu, C.; Webb, W. W. *J. Opt. Soc. Am. B* **1996**, *13*, 481–491.
(45) Albota, M.; Beljonne, D.; Bredas, J.-L.; Ehrlich, J. E.; Fu, J.-Y.; Heikal, A. A.; Hess, S. E.; Kogej, T.; Levin, M. D.; Marder, S. R.; McCord-Maughon, D.; Perry, J. W.; Rockel, H.; Rumi, M.; Subramaniam, C.; Webb, W. W.; Wu, X.-L.; Xu, C. *Science* **1998**, *281*, 1653–1656.
(46) (a) Yang, N. C.; Lee, S. M.; Yoo, Y. M.; Kim, J. K.; Suh, D. H. *J. Polym. Sci., Part A: Polym. Chem.* **2004**, *42*, 1058–1068. (b) Ding, J.; Day, M.; Robertson, G.; Roovers, J. *Macromolecules* **2002**, *35*, 3474–3483.
(47) (a) Takahashi, S.; Kuroyama, Y.; Sonogashira, K.; Hagihara, N. *Synthesis* **1980**, 627–630. (b) Lewis, J.; Long, N. J.; Raithby, P. R.; Shields, G. P.; Wong, W. Y.; Younus, M. *J. Chem. Soc., Dalton Trans.* **1997**, 4283–4288.
(48) (a) Wong, W.-Y.; Ho, C.-L. *Coord. Chem. Rev.* **2006**, *250*, 2627–2690. (b) Wong, W.-Y. *Dalton Trans.* **2007**, 4495–4510. (c) Wong, W.-Y. *J. Inorg. Organomet. Polym. Mater.* **2005**, *15*, 197–219.
(49) (a) Wittmann, H. F.; Friend, R. H.; Khan, M. S.; Lewis, J. *J. Chem. Phys.* **1994**, *101*, 2693–2698. (b) Chawdhury, N.; Köhler, A.; Friend, R. H.;

Wong, W.-Y.; Lewis, J.; Younus, M.; Raithby, P. R.; Corcoran, T. C.; Al-Mandhary, M. R. A.; Khan, M. S. *J. Chem. Phys.* **1999**, *110*, 4963–2698.
(50) Wilson, J. S.; Chawdhury, N.; Al-Mandhary, M. R. A.; Younus, M.; Khan, M. S.; Raithby, P. R.; Köhler, A.; Friend, R. H. *J. Am. Chem. Soc.* **2001**, *123*, 9412–9417.
(51) (a) Hertel, D.; Setayesh, S.; Nothofer, H. G.; Scherf, U.; Müllen, K.; Bässler, H. *Adv. Mater.* **2001**, *13*, 65–70. (b) Monkman, A. P.; Burrows, H. D.; Hartwell, L. J.; Horsburgh, I. E.; Hamblett, I.; Navaratnam, S. *Phys. Rev. Lett.* **2001**, *86*, 1358–1361.
(52) Wilson, J. S.; Köhler, A.; Friend, R. H.; Al-Suti, M. K.; Al-Mandhary, M. R. A.; Khan, M. S.; Raithby, P. R. *J. Chem. Phys.* **2000**, *113*, 7627–7634.
(53) A description of the heavy atom effect and the effect of molecular size on the nonradiative internal conversion rate constants (also called loose bolt effect) can be found in Turro, N. J. *Modern Molecular Photochemistry*; University Science Books: Sausalito, CA, 1991 and in Turro, N. J.; Ramamurthy, V.; Scaiano, J. C. *Modern Molecular Photochemistry of Organic Molecules*; University Science Books: New York, 2010. Moreover, other examples where the excited-state lifetimes decrease with the molecular size of oligomers can be found in (a) Liu, L.; Fortin, D.; Harvey, P. D. *Inorg. Chem.* **2009**, *48*, 5891–5900. (b) Jiang, F.-L.; Fortin, D.; Harvey, P. D. *Inorg. Chem.* **2010**, *49*, 2614–2623.
(54) (a) Ramakrishna, G.; Goodson, T., III. *J. Phys. Chem. A* **2007**, *111*, 993–1000. (b) Fouassier, J.-P.; Lougnot, D. J.; Wieder, F.; Faure, J. *J. Photochem.* **1977**, *7*, 17–28.
(55) Rulliere, C.; Rayez, J.-C.; Roberge, P. C. *Can. J. Chem.* **1978**, *56*, 2781–2785.
(56) Westlund, R.; Glimsdal, E.; Lindgren, M.; Vestberg, R.; Hawker, C.; Lopez, C.; Malmström, E. *J. Mater. Chem.* **2008**, *18*, 166–170.
(57) (a) McKay, T. J.; Staromlynska, J.; Wilson, P. *J. Appl. Phys.* **1999**, *85*, 1337–1341. (b) Glimsdal, E.; Carlsson, M.; Eliasson, B.; Minaev, B.; Lindgren, M. *J. Phys. Chem. A* **2007**, *111*, 244–250.
(58) Rogers, J. E.; Slagle, J. E.; Krein, D. M.; Durke, A. R.; Hall, B. C.; Fratini, A.; McLean, D. G.; Fleitz, P. A.; Cooper, T. M.; Drobizhev, M.; Makarov, N. S.; Rebane, A.; Kim, K.-Y.; Farley, R.; Schanze, K. S. *Inorg. Chem.* **2007**, *46*, 6483–6494.
(59) Hughes, G.; Bryce, M. R. *J. Mater. Chem.* **2005**, *15*, 94–107.
(60) (a) Blom, P. W. M.; de Jong, M. J. M.; Liedenbaum, T. H. F. *Polym. Adv. Tech.* **1998**, *9*, 390–401. (b) Friend, R. H.; Greenham, N. C. In *Handbook of Conducting Polymers*, 2nd ed.; Skotheim, T. A., Elsenbaumer, R. L., Reynolds, J. R., Eds.; Marcel Dekker: New York, 1998; p823.
(61) (a) Zhan, X.; Liu, Y.; Wu, X.; Wang, S.; Zhu, D. *Macromolecules* **2002**, *35*, 2529–2537. (b) Kraft, A.; Grimsdale, A. C.; Holmes, A. B. *Angew. Chem., Int. Ed.* **1998**, *37*, 402–428.
(62) (a) Zhou, G.; Ho, C.-L.; Wong, W.-Y.; Wang, Q.; Ma, D.; Wang, L.; Lin, Z.; Marder, T. B.; Beeby, A. *Adv. Funct. Mater.* **2008**, *18*, 499–511. (b) Ho, C.-L.; Wong, W.-Y.; Zhou, G.-J.; Yao, B.; Xie, Z.; Wang, L. *Adv. Funct. Mater.* **2007**, *17*, 2925–2936. (c) Ho, C.-L.; Wong, W.-Y.; Gao, Z.-Q.; Chen, C.-H.; Cheah, K.-W.; Yao, B.; Xie, Z.; Wang, Q.; Ma, D.; Wang, L.; Yu, X.-M.; Kwok, H.-S.; Lin, Z. *Adv. Funct. Mater.* **2008**, *18*, 319–331.
(63) Wong, W.-Y.; Zhou, G.-J.; Yu, X.-M.; Kwok, H.-S.; Tang, B.-Z. *Adv. Funct. Mater.* **2006**, *16*, 838–846.
(64) Qian, L.; Yang, S. Y.; Jin, Z. S.; Zhang, Z. J.; Zhang, T.; Teng, F.; Xu, X. R. *Phys. Lett. A* **2005**, *335*, 56–60.
(65) Wu, H.; Zhou, G.; Zou, J.; Ho, C.-L.; Wong, W.-Y.; Yang, W.; Peng, J.; Cao, Y. *Adv. Mater.* **2009**, *21*, 4181–4184.
(66) Gong, X.; Lim, S.-H.; Ostrowski, J. C.; Moses, D.; Bardeen, C. J.; Bazan, G. C. *J. Appl. Phys.* **2004**, *95*, 948–953.
(67) Kang, J.-W.; Lee, D.-S.; Park, H.-D.; Park, Y.-S.; Kim, J. W.; Jeong, W.-I.; Yoo, K.-M.; Go, K.; Kim, S.-H.; Kim, J.-J. *J. Mater. Chem.* **2007**, *17*, 3714–3719.
(68) Paik, K. L.; Baek, N. S.; Kim, H. K.; Lee, J.-H.; Lee, Y. *Macromolecules* **2002**, *35*, 6782–6791.
(69) Sun, M.; Zhong, C.; Li, F.; Cao, Y.; Pei, Q. *Macromolecules* **2010**, *43*, 1714–1718.
(70) (a) Aly, S. M.; Ho, C.-L.; Wong, W.-Y.; Abd-El-Aziz, A. S.; Harvey, P. D. *Chem.—Eur. J.* **2008**, *14*, 8341–8352. (b) Aly, S. M.; Ho, C.-L.; Wong, W.-Y.; Fortin, D.; Harvey, P. D. *Macromolecules* **2009**, *42*, 6902–6916.